INVESTIGATION OF ELECTRONIC TRANSPORT, RECOMBINATION AND OPTICAL PROPERTIES IN InAs(1-x)P(x) ALLOY SYSTEMS

Sheng S. Li

Florida University

Prepared for:

Army Night Vision Laboratory
Defense Advanced Research Project Agency

15 June 1975

University of Florida

Gainesville, Florida

INVESTIGATION OF ELECTRONIC TRANSPORT, RECOMBINATION AND OPTICAL PROPERTIES IN $InAs_{1-x}P_x$ ALLOY SYSTEMS

THIRD SEMI-ANNUAL TECHNICAL REPORT
(December 1974 - May 1975)

Sheng S. Li, Principal Investigator
Tel. (904) 392-4927

June 15, 1975

NIGHT VISION LABORATORY
U.S. ARMY ELECTRONICS COMMAND
FORT BELVOIR, VIRGINIA 22060

SPONSORED BY
ADVANCED RESEARCH PROJECTS AGENCY
ARPA ORDER 2182
PROGRAM CODE 4D10
CONTRACT DAAK02-74-C-0102

Effective Date: December 1, 1973
Expiration: November 30, 1975

Electron Device Research Center

College of Engineering

INVESTIGATION OF ELECTRONIC TRANSPORT, RECOMBINATION AND OPTICAL PROPERTIES IN $InAs_{1-x}P_x$ ALLOY SYSTEMS

THIRD SEMI-ANNUAL TECHNICAL REPORT
(December 1974 - May 1975)

Sheng S. Li, Principal Investigator
Tel. (904) 392-4927

June 15, 1975

NIGHT VISION LABORATORY
U.S. ARMY ELECTRONICS COMMAND
FORT BELVOIR, VIRGINIA 22060

SPONSORED BY
ADVANCED RESEARCH PROJECTS AGENCY
ARPA ORDER 2182
PROGRAM CODE 4D10
CONTRACT DAAK02-74-C-0102

Effective Date: December 1, 1973
Expiration: November 30, 1975

Electron Device Research Center
Department of Electrical Engineering
University of Florida
Gainesville, Florida 32611

REPORT DOCUMENTATION PAGE

READ INSTRUCTIONS BEFORE COMPLETING FORM

1. REPORT NUMBER: Progress Report No. 3	2. GOVT ACCESSION NO.
3. RECIPIENT'S CATALOG NUMBER	
4. TITLE (and Subtitle): Investigation of the Electronic Transport and Optical Properties in $InAs_{1-x}P_x$ Alloy Systems	5. TYPE OF REPORT & PERIOD COVERED: 3rd Semi-Annual Technical; January-June 1975
	6. PERFORMING ORG. REPORT NUMBER
7. AUTHOR(s): Sheng S. Li	8. CONTRACT OR GRANT NUMBER(s): DAAK02-74-C-0102
9. PERFORMING ORGANIZATION NAME AND ADDRESS: University of Florida, Engineering & Industrial Experiment Station, Gainesville, FLA 32611	10. PROGRAM ELEMENT, PROJECT, TASK AREA & WORK UNIT NUMBERS: 2182, n/a, n/a; 4D10; DOD Supplement
11. CONTROLLING OFFICE NAME AND ADDRESS	12. REPORT DATE: June 30 1975
	13. NUMBER OF PAGES: 73
14. MONITORING AGENCY NAME & ADDRESS (if different from Controlling Office): Night Vision Laboratory, U.S. Army Electronics Command, Fort Belvoir, Virginia 22060	15. SECURITY CLASS. (of this report): unclassified
	15a. DECLASSIFICATION/DOWNGRADING SCHEDULE

16. DISTRIBUTION STATEMENT (of this Report)

Approved for public release; distribution unlimited.

17. DISTRIBUTION STATEMENT (of the abstract entered in Block 20, if different from Report)

18. SUPPLEMENTARY NOTES

This research was supported by the Defense Advanced Research Project Agency.

19. KEY WORDS (Continue on reverse side if necessary and identify by block number)

$InAs_{1-x}P_x$ epitaxial films, resistivity, Hall coefficient, impurity conduction, electron mobility, electron concentration, magnetoresistance coefficient, optical absorption coefficient, minority carrier diffusion length, surface photovoltage, electron microprobe analysis.

20. ABSTRACT (Continue on reverse side if necessary and identify by block number)

Measurements of the electrical resistivity, the Hall coefficient and the magnetoresistance as functions of temperature have been carried out for seven $InAs_{0.63}P_{0.37}$ epitaxial samples 172-179 with film thicknesses varying from 2.35 to 4.3 μm. The results yielded electron mobility and electron concentration as functions of the H_2 flow-rate and the temperature between 4.2°K and 300°K. The electron mobility for this set of samples, was

DD FORM 1 JAN 73 1473 EDITION OF 1 NOV 65 IS OBSOLETE S/N 0102-014-6601

unclassified

SECURITY CLASSIFICATION OF THIS PAGE (When Data Entered)

20. (cont'd.)
found to be lower than the mobility for samples 164-171 reported previously.[1] Concluding remarks concerning the conduction processes in the InAsP epitaxial samples are given. The conduction processes can be characterized by the expression

$$\sigma(T) = C_1 \exp\left(-\frac{E_1}{kT}\right) + C_2(T) \quad ,$$

where E_1 is the normal donor ionization energy and the second term represents the linear region observed in the lower temperature zone.

Optical absorption coefficients for samples 172-178 have been deduced from transmission measurements near the fundamental absorption edge. The alloy compositions for 14 $InAs_{1-x}P_x$ epitaxial samples are deduced from the electron microprobe analysis.

Surface photovoltage (SPV) measurements for determining the minority carrier diffusion length in the InAsP bulk and epitaxial samples are described; SPV theory is reviewed.

FOREWORD

This technical report covers research activities carried out between January and June 1975 under contract DAAK02-74-C-0102. Mr. Terry Jones (AMSEL-NV-II) is the responsible Army Night Vision Laboratory Contract Monitor. This work was performed in the Department of Electrical Engineering of the University of Florida, Gainesville, Florida. The principal investigator for this research project is Dr. Sheng S. Li. Major contributors include S. S. Li, J. R. Anderson, D. W. Schoenfeld and R. A. Owen. The author is grateful to Dr. J. K. Kennedy of the Air Force Cambridge Research Laboratory, who so generously prepared for us the $InAs_{1-x}P_x$ epitaxial samples used in this research project.

ABSTRACT

The research program sponsored by this contract during the fifth and sixth quarters has produced technical findings in several areas: (1) Electron microprobe analysis on fourteen $InAs_{1-x}P_x$ epitaxial samples (of thicknesses ranging from 14.6 μm to 2.35 μm) has yielded information in areas such as atomic compositions, the epitaxial layer homogeneity and the epilayer thickness. (2) Resistivity, Hall effect and magnetoresistance measurements on seven $InAs_{10.63}P_{0.37}$ epitaxial samples (172-178) have yielded information about both electron mobility and electron concentration as functions of the temperature and the H_2 flow rate. Conclusions concerning the conduction processes and the scattering mechanisms in InAsP alloy systems are given. (3) The optical absorption coefficient as a function of wavelength, deduced from transmission measurements, is given for seven InAsP epitaxial samples (172-178). (4) The surface photovoltage (SPV) method for determining the minority carrier diffusion length, in both bulk and epitaxial semiconductor specimens, is described.

TABLE OF CONTENTS

FIGURE CAPTIONS

LIST OF TABLES

I. INTRODUCTION

This third semi-annual technical report covers research activities from January to June 1975.

The general research goals for this project were to conduct theoretical and experimental studies of the basic electronic transport, recombination, optical and structural properties in both bulk and epitaxial $InAs_{1-x}P_x$ alloy systems, for the 1~2 μm infrared (IR) photocathode and for other IR devices and system applications.

Specific physical parameters to be determined from this research program include: (1) electron mobility and concentration as functions of the alloy composition, the H_2 carrier gas flow rate, and the temperature, (2) optical absorption coefficient as a function of the alloy composition and the wavelength, (3) energy band gap versus the alloy composition, (4) density and activation energy of the impurities and defects, (5) the minority carrier diffusion length and lifetime, (6) the interrelations between the aforementioned parameters and the epitaxial growth parameters (such as the H_2 flow rate), and (7) the conduction processes, and recombination and scattering mechanisms.

Experimental tools employed include: (1) electron microprobe analysis, (2) resistivity and Hall effect measurements, (3) low temperature ac conductivity measurements, (4) magnetoresistance measurements, (5) optical transmission and reflectance measurement, (6) surface photovoltage measurement, and (7) photoconductivity and photomagnetoelectric effect measurements.

Major achievements derived during this reporting period include:

(A) Preparation of Seven InAsP Epitaxial Samples:

During this reporting period, seven additional samples of $InAs_{0.61}P_{0.39}$ epitaxial films were prepared at the Air Force Cambridge Research Laboratory. Four of these samples, InAsP-196, 197, 181 and 186, were deposited on semi-insulating Cr-doped GaAs substrate. The remaining three samples, InAsP-198, 199 and 200, were deposited on p-type InAs substrates, which have a carrier concentration of approximately $1 \times 10^{17} cm^{-3}$. All flow parameters, except the H_2 flow rate, were identical to the previous samples[1]. The deposition time for these samples, however, was four hours. The H_2 flow rates used for each sample and the estimated thicknesses are listed in Table 1.1.

(B) Electron Microprobe Studies:

Electron microprobe analysis was performed on fourteen $InAs_{1-x}P_x$ epitaxial samples (164-178). The alloy compositions (i.e., the atomic percentage of indium, arsenic and phosphorus), the epitaxial layer thicknesses, and the homogeneities of the epilayers were determined and analyzed for these samples. The results of this analysis are listed in Table 2.1. The average epilayer thickness for samples 164-171 is 14 μm, compared with 3.6 μm for samples 172-178.

(C) Resistivity and Hall Coefficient Data:

Resistivity and Hall effect measurements were conducted for $InAs_{0.63}P_{0.37}$ epitaxial samples 172 through 178, as functions of the temperature (between 4.2°K and 300°K) and the H_2 flow rate.

The electron mobility and concentration were deduced from these measurements. It was found that the electron mobility for this set of samples (with epilayer thicknesses varying from 4.5 μm to 2.35 μm) is considerably lower than that of samples 164-171 reported previously[1]. This is particularly evident for samples 177 and 178 (2 μm film), where the room temperature mobility is found to be less than 3000 $cm^2/V\text{-}s$. The reduction in electron mobility with decreasing film thickness is believed to be due to lattice mismatching and the nonstochiometric crystal structure existing in these two samples. Concluding remarks concerning the conduction processes in the InAsP alloy systems are given in this report.

(D) Magnetoresistance Data

The magnetoresistance, as a function of the magnetic flux density for sample 172 through 178, was measured at T = 77°K and 4.2°K. The results show that the magnetoresistance ($\Delta\rho/\rho_o$) is directly proportional to the square of the magnetic flux density (B^2), for weak magnetic fields at 77°K. However, negative magnetoresistance was observed for T = 4.2°K and was attributed to the impurity conduction process taking place at this low temperature. The magnetoresistance coefficient deduced at 77°K further indicates that ionized impurity scattering prevails for these samples in this temperature range.

(E) Optical Transmission and Surface Photovoltage Measurements

Optical transmission and surface photovoltage measurements were performed for InAsP epitaxial samples 172 through 178. Optical absorption coefficient as a function of wavelength was

deduced from transmission data for samples 172 through 178 near the fundamental absorption edge. The energy band gap determined for this set of samples varied from 0.582 eV to 0.596 eV with $\alpha = 10^3 cm^{-1}$.

The surface photovoltage (SPV) method was used to determine the minority carrier diffusion length in InAsP samples. SPV theory and its experimental setup are described.

TABLE 1.1 $InAs_{0.61}P_{0.39}$ epitaxial samples to be used for transport and optical properties study.

Sample #	H_2 Flow Rate (cc/min)	Estimated Thickness (μm)	Substrate
196	3070	94	semi-insulating GaAs substrate
197	2430	87	
181	1780	78	
186	1530	77	
198	2430	110	p-type InAs substrate
199	1280	73	
200	730	52	

II. ELECTRON MICROPROBE ANALYSIS (EMA)

During this contract reporting period, our electron microprobe studies have been directed towards the investigation of the alloy composition, epitaxial layer thickness, and homogeneity of the fourteen $InAs_{1-x}P_x$ epitaxial samples (164-171 and 172-178). As described in our previous technical report[1], these epitaxial films were grown on semi-insulating, Cr-doped GaAs substrates. The AsH_3/PH_3 ratio used was identical to that used in growing $InAs_{0.69}P_{0.31}$ epitaxial samples 153-159[2].

All growth parameters, except the hydrogen carrier gas flow-rate, were held constant. The deposition time for samples 164, and 166 to 171 was 20 minutes, and the H_2 flow rate varied from 1780 cc/min. to 515 cc/min. For samples 172 to 178, the deposition times was 6 minutes. The resulting epitaxial layer thickness and atomic composition are summarized in Table 2.1.

The epilayer thicknesses vary from 14.6 μm for sample 164, to 2.3 μm for 178. The average alloy composition for samples 164-171 is $InAs_{0.55}P_{0.45}$ (i.e., 55% InAs and 45% InP). For samples 172-178, the result yields $InAs_{0.63}P_{0.37}$ (i.e., 63% InAs and 37% InP).

It is worth noting that the electron microprobe technique appears to be unsuitable for determining the film thickness and for analyzing the homogeneity of the film for epitaxial layer thickness less than 4 μm. This is because the secondary fluorescence effect and the x-ray

beam size at the boundary layer of the epifilm and the substrate become very critical for the thin epitaxial samples, such as samples 177 and 178. As a result, the present electron microprobe analysis leaves some uncertainty over the data on atomic composition and epilayer thickness.

2.1 Sample Preparation

As described in our previous technical report[1], samples used for EMA were first plated with nickel films to protect the epitaxial layer edges from rounding during polishing. Next the samples were embedded in copper-filled DIALLYL PHTHALATE. The samples were then polished and ready for EMA.

Sample polishing was performed by using the IMACO multipol precision polishing machine. The only change in the previously outlined polishing procedures[1] was that a politex supreme poromeric polishing cloth and a water-based abrasive slurry were used in place of the Buehler microcloth and glycerine mixed slurry. The ability to repeatedly obtain a flat polishing surface was substantially increased over previous efforts.

Details of EMA were described in our previous report[1-2]. For the present report, the EMA procedures are described briefly as follows. Line graphs of the characteristic x-ray intensities for Indium $L_{\alpha 1}$, arsenic K_{α}, and phosphorus K_{α}, using an accelerating voltage of 15 KV, were obtained by scanning the cross section of each of the fourteen samples and then recorded by using a strip chart recorder.

The mean atomic composition was calculated by using the MAGIC IV computer program for quantitative microprobe analysis. The results were tabulated in Table 2.1 for fourteen InAsP epitaxial samples.

2.2 Results for Samples 164-178

The atomic percentages of In, As and P for the first set of $InAs_{1-x}P_x$ epitaxial samples 164-171 (as deduced from EMA described in Section 2.1) are shown, respectively, in Fig. 2.1 a through Fig. 2.1 g. The relative x-ray intensities from each element (i.e., In, As and P) are plotted as a function of distance from the substrate across the epitaxial layer and the nickel plating layer. These results are similar to those we had observed previously[1] for samples 153-159 (except the thickness of the epilayer was changed). The average alloy composition for this set of samples was determined from the graphs, and the result was found to be $InAs_{0.55}P_{0.45}$. For film thicknesses in excess of 10 μm (e.g., samples 164 through 170), it was found that the EMA proved to be an effective tool in determining the thickness, alloy composition and homogeneity of the epitaxial layer of each of these InAsP samples. However, for epilayer thicknesses less than 5 μm, the EMA results are somewhat uncertain and inconclusive. This is the case for our epitaxial samples 171 through 178, in which all the epilayer thicknesses are less than 5 μm.

The EMA results for the atomic compositions of seven $InAs_{1-x}P_x$ epitaxial samples, 172 through 178, are displayed in Fig. 2.2 a through Fig. 2.2 g. From these figures, it is noted that the boundary between the substrate and the epilayer is not

well defined; the transition in x-ray intensity for each constituent element (i.e., In, As and P) is gradual as it crosses the interfacial layer. This occurs because the electron beam size (i.e., order of micron) and the effects of the secondary fluorescence, near the transition region of the substrate and the epilayer, are significant for these thin samples. As a result, no conclusion can be deduced from the EMA for this set of samples.

An estimation of the average alloy composition for samples 172 through 178 was made from the EMA data, and the result yielded an average value of $InAs_{0.63}P_{0.37}$. This is in good agreement with the alloy composition prescribed for this set of samples, and with our previous samples, 153 through 159[1].

It is worth noting that the two thinnest samples, 177 and 178 of this set, showed an anomalously low indium content (~31%), implying highly nonstochiometric crystal structure. As a result, very low electron mobility and high electron concentration are observed for these two samples. These findings will be discussed in Chapter III.

The atomic composition of the samples (i.e., the proportions of In, As and P) varies with the H_2 carrier gas flow rate and the homogeneity of these epitaxial films. The variation is illustrated in Fig. 2.4 through Fig. 2.6. The epitaxial layer thickness versus the H_2 flow-rate for samples 172 through 178 is shown in Fig. 2.3. The epitaxial film thicknesses were found to vary from 4.35 μm to about 2.3 μm, as the H_2 flow rate changed from 1780 cc/min to 515 cc/min. The two thinnest samples (177-178) show poor structural and

electrical characteristics. These will be discussed in Chapter III.

Fig. 2.4 through Fig. 2.6 show the alloy composition and atomic percentages versus the H_2 flow rate for samples 164-171 and 172-178. The results indicate that in the thicker films (i.e., samples 164-171), the atomic composition shows a higher degree of uniformity from sample to sample and less variation with H_2 flow rate than in the thinner samples (i.e., 172-178). The results further show that at low flow rates there are lower indium atomic percentages in the thin samples (i.e., 177-178) than in the thick samples. This implies that nonstochiometric structure is a principal problem for these thin samples. This, in turn, affects the electron mobility and carrier concentration in these specimens, a topic to be discussed later in this report.

2.3 Summary

Electron Microprobe Analysis (EMA) has been made for two sets of InAsP epitaxial samples: samples 164 through 171, and samples 172 through 178. The average epilayer thickness was 14 μm for samples 164 through 171, and 3.6 μm for samples 172 through 178. The average alloy composition was 55% InAs and 45% InP (i.e., $InAs_{0.55}P_{0.45}$) for samples 164 through 171, and 63% InAs and 37% InP (i.e., $InAs_{0.63}P_{0.37}$) for samples 172 through 178. Relative homogeneity across the epilayer was observed for samples 164 through 170. However, the EMA could not conclusively determine the epilayer homogeneity or thickness of samples 171-178 because of insufficient beam resolution and secondary fluorescence effects. The anomalous

EMA results (low indium contents) for samples 177 and 178 indicate that the epilayers in these two samples are of low quality, as is reflected by their low electron mobility and high electron concentration. These characteristics will be discussed in Chapter III.

TABLE 2.1 Atomic composition and epitaxial layer thickness for 14 $InAs_{1-x}P_x$ epitaxial samples, as determined from Electron Microprobe Analysis.

Sample No.	H_2 flow rate (cc/min)	Atomic percentage (%)			$InAs_{1-x}P_x$ x	Epilayer thickness(μm)*
		In	As	P		
164	1780	51.41	25.67	22.92	0.472	14.64
166	1280	52.06	28.42	19.52	0.407	14.56
167	730	49.97	28.67	21.37	0.427	13.33
168	1530	49.85	27.98	22.17	0.442	
169	910	49.93	27.37	22.70	0.453	13.01
170	570	53.96	23.99	22.05	0.489	14.61
171	515	51.50	25.14	23.37	0.482	6.88
172	1780	50.38	30.65	18.97	0.618	4.25
173	1530	42.47	34.95	22.58	0.599	4.15
174	1280	44.51	37.01	18.48	0.667	4.10
175	910	52.22	29.98	17.79	0.628	3.65
176	730	41.34	37.02	21.63	0.651	2.82
177	570	31.47	40.81	27.27	0.596	2.63
178	515	30.62	44.22	25.17	0.637	2.35

*Determined by optical microscope method.

Fig. 2.1 (a) through (g) Relative x-ray intensity from indium, arsenic and phosphorus as recorded from the scanning of the electron microprobe across the substrate, the epilayer and the nickel plated layer for samples 164 through 171.

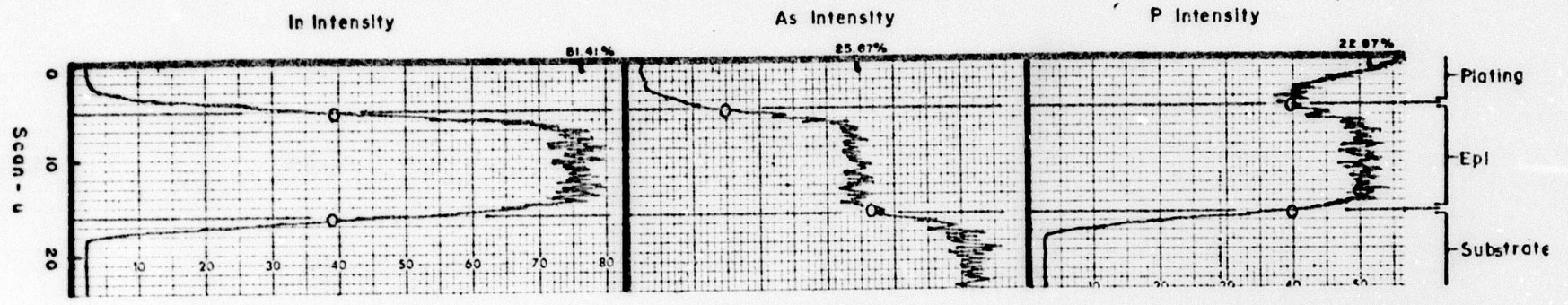

SAMPLE No. 164

Fig. 2.1(a)

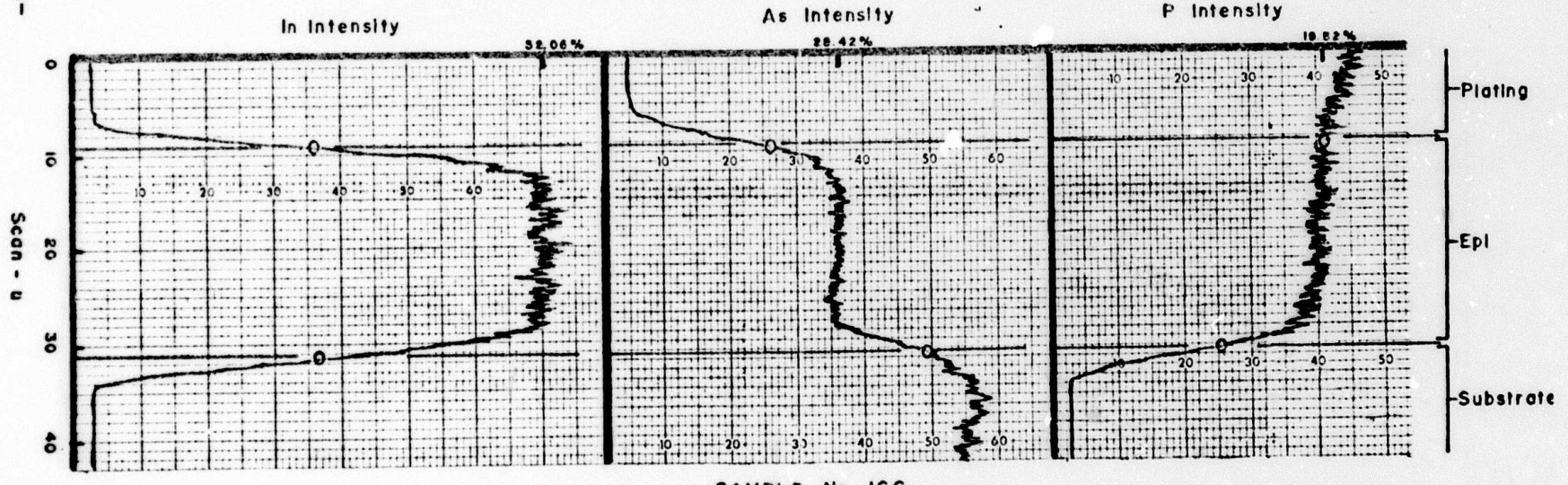

SAMPLE No. 166

Fig. 2.1(b)

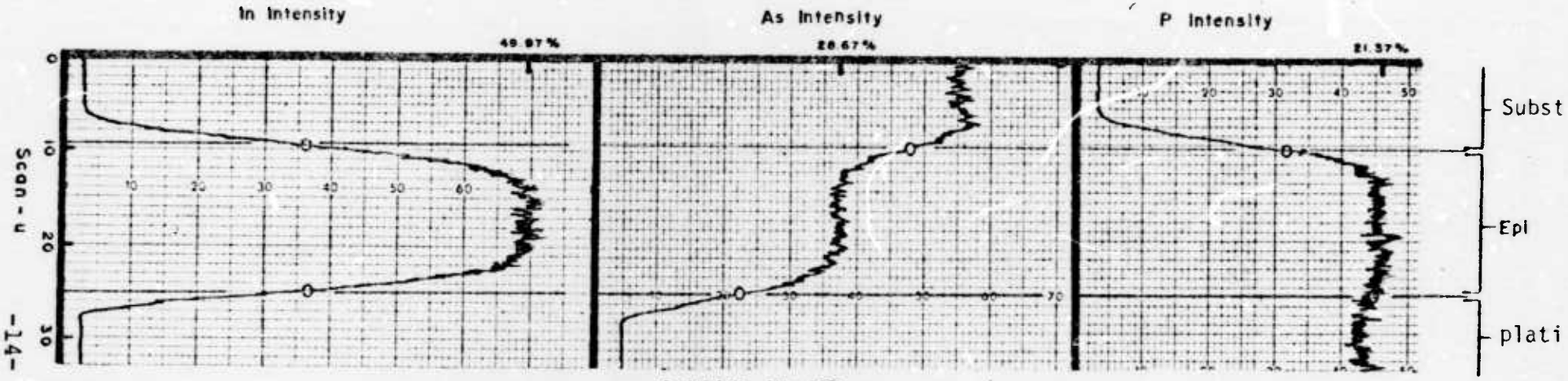

SAMPLE No. 167

Fig. 2.1(c)

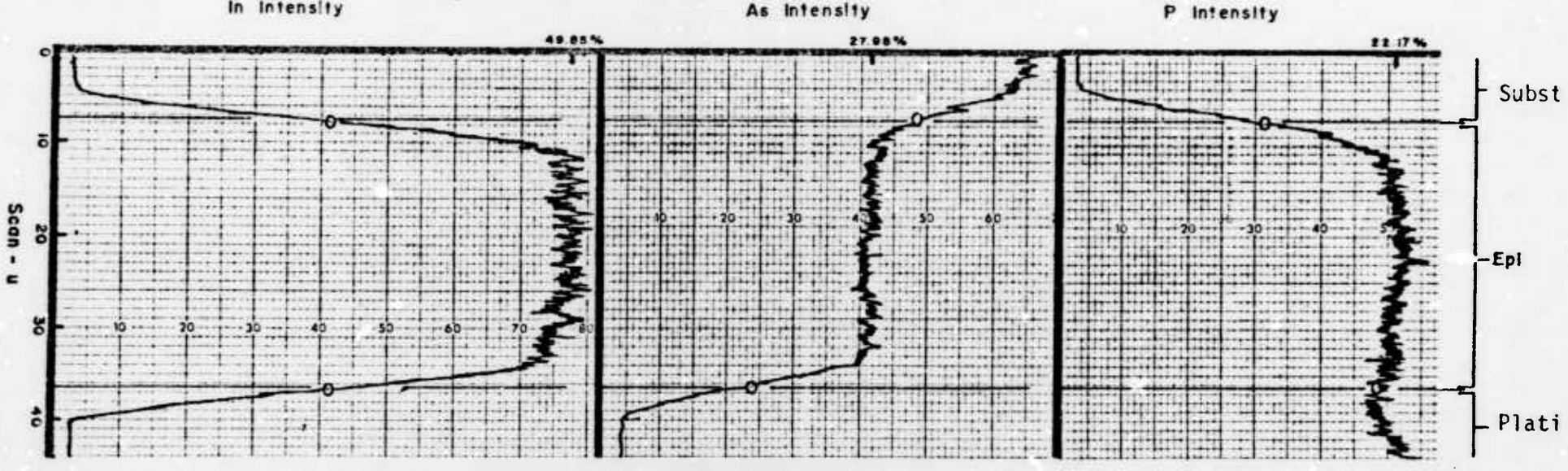

SAMPLE No. 168

Fig. 2.1(d)

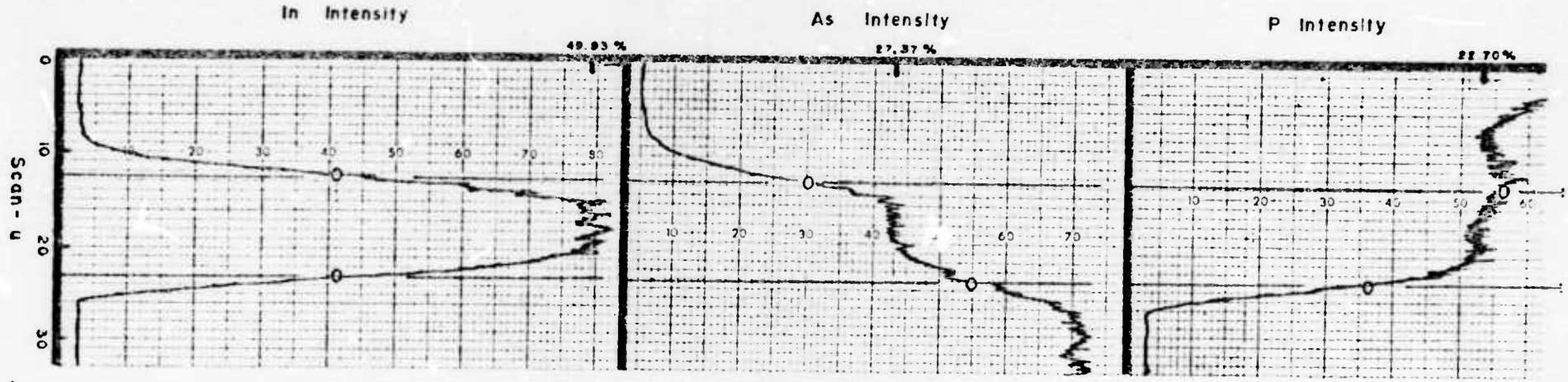

SAMPLE No 169

Fig. 2.1(e)

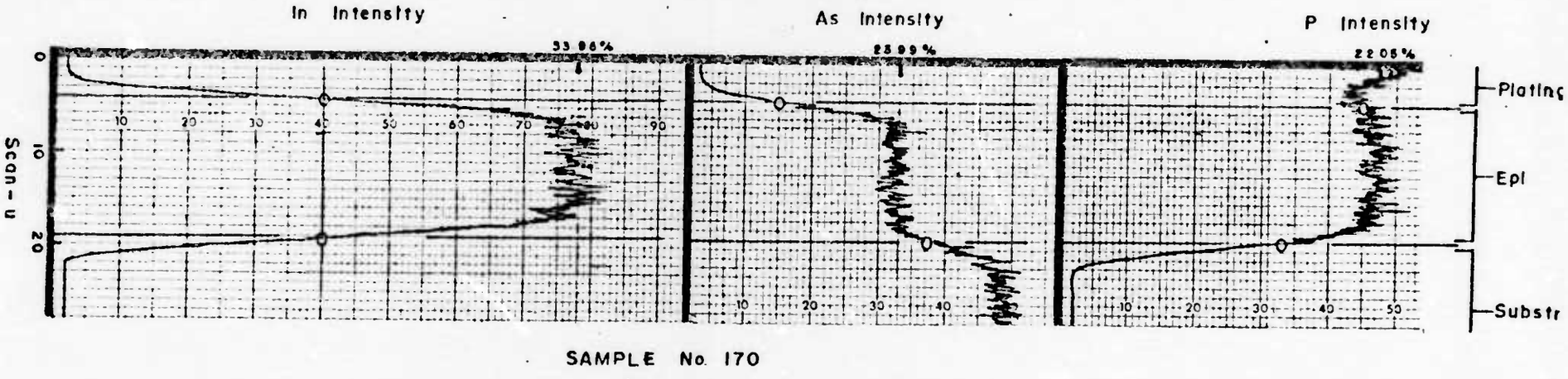

SAMPLE No. 170

Fig. 2.1(f)

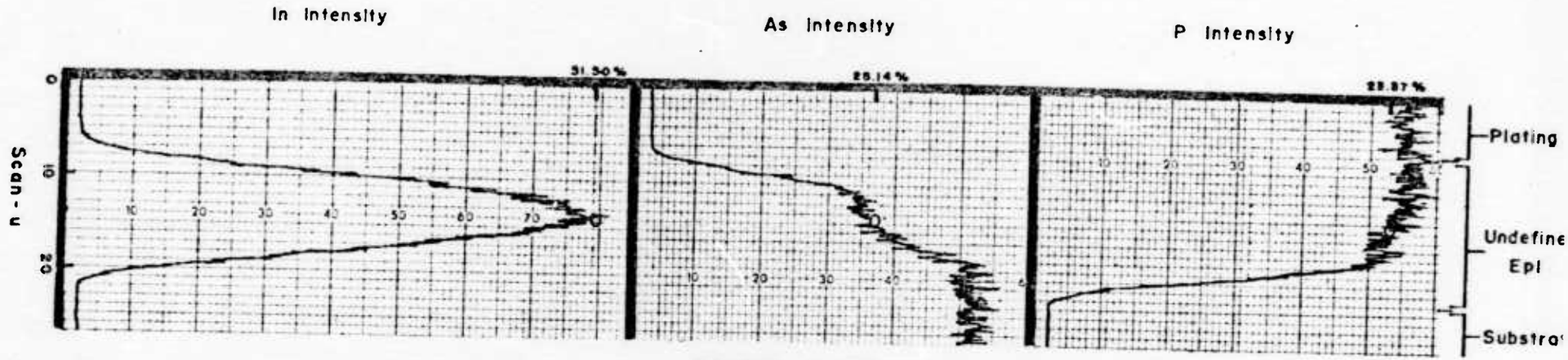

SAMPLE No. 171

Fig. 2.1(g)

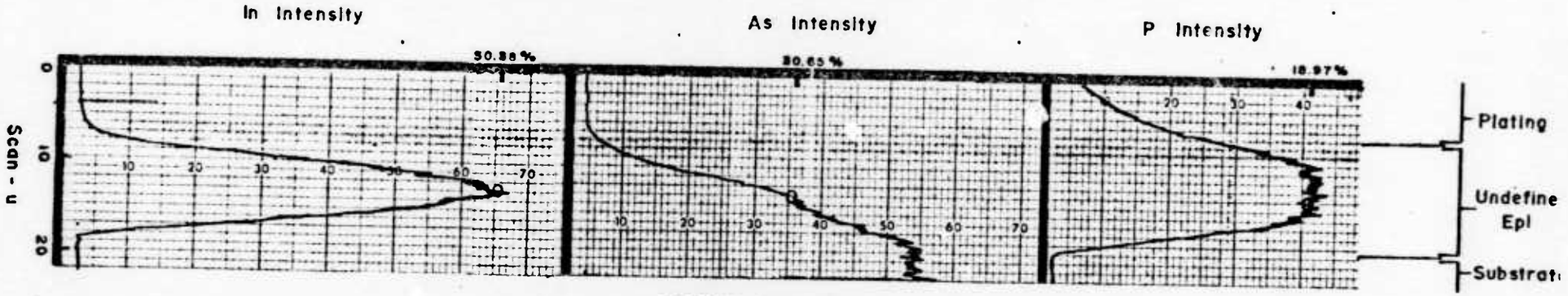

SAMPLE No. 172

Fig. 2.2(a)

Fig. 2.2 (a) through (g) Shows the relative x-ray intensity from indium, arsenic and phosphorus as recorded from the scanning of the electron microprobe across the substrate, the epilayer and the nickel plated layer for samples 172 through 178.

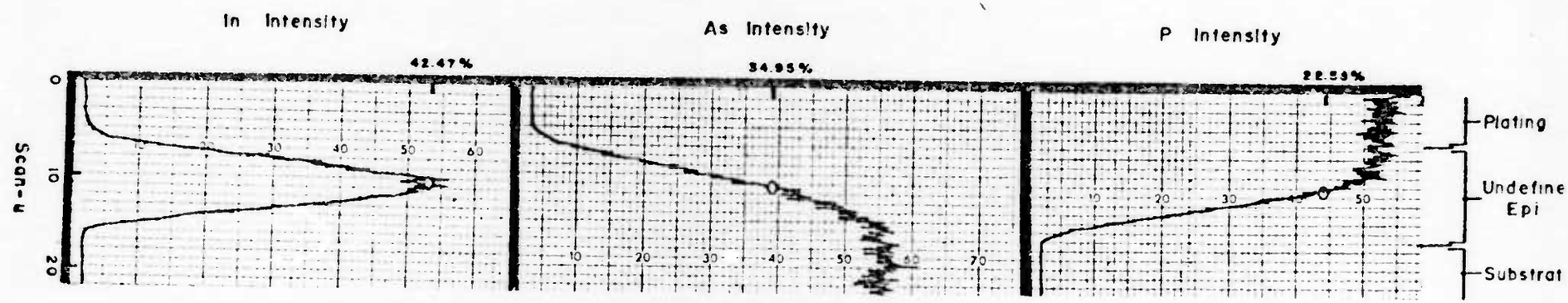

SAMPLE No. 173

Fig. 2.2(b)

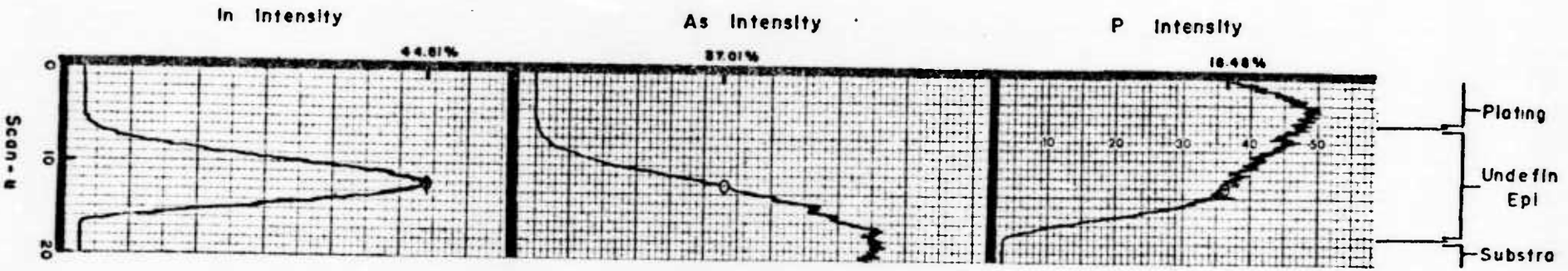

SAMPLE No. 174

Fig. 2.2(c)

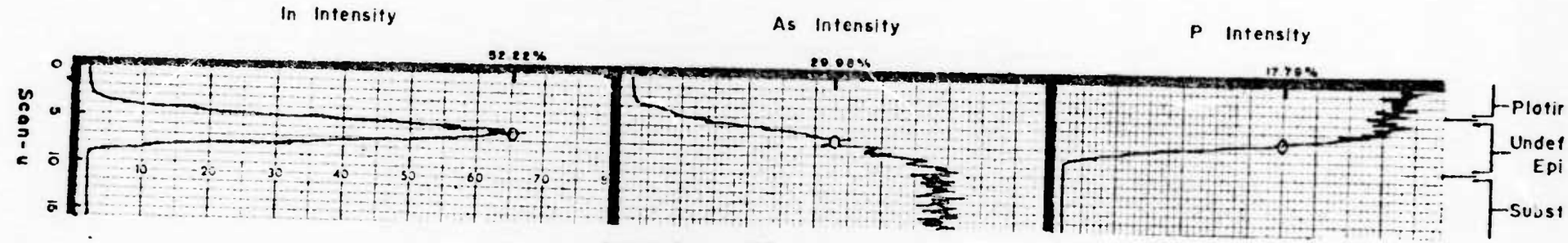

SAMPLE No. 175

Fig. 2.2(d)

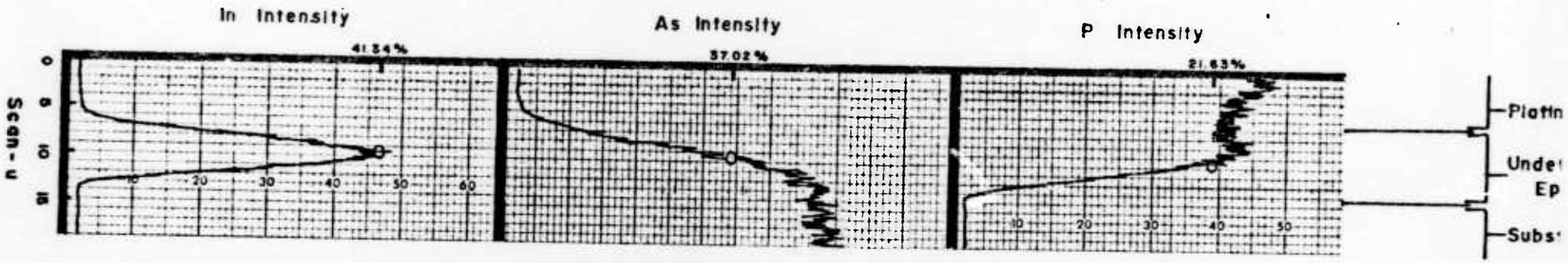

SAMPLE No. 176

Fig. 2.2(e)

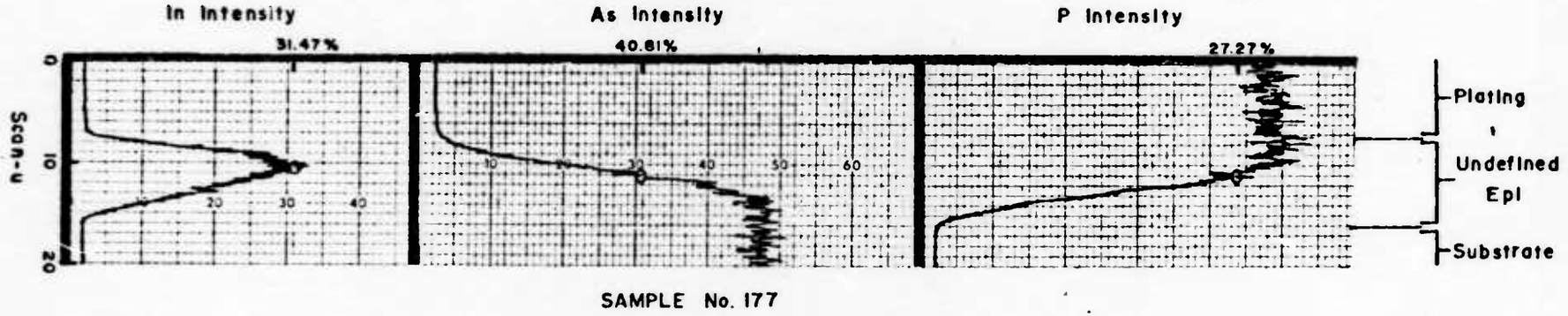

SAMPLE No. 177

Fig. 2.2(f)

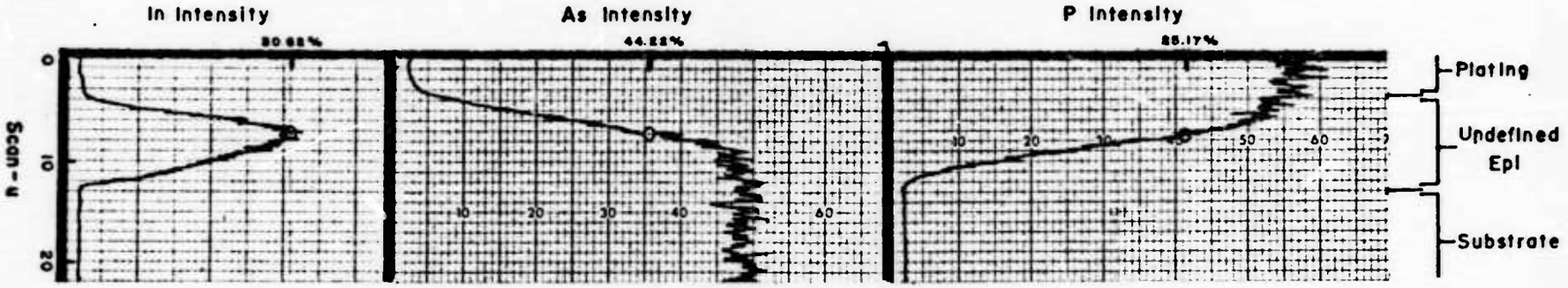

SAMPLE No. 178

Fig. 2.2(g)

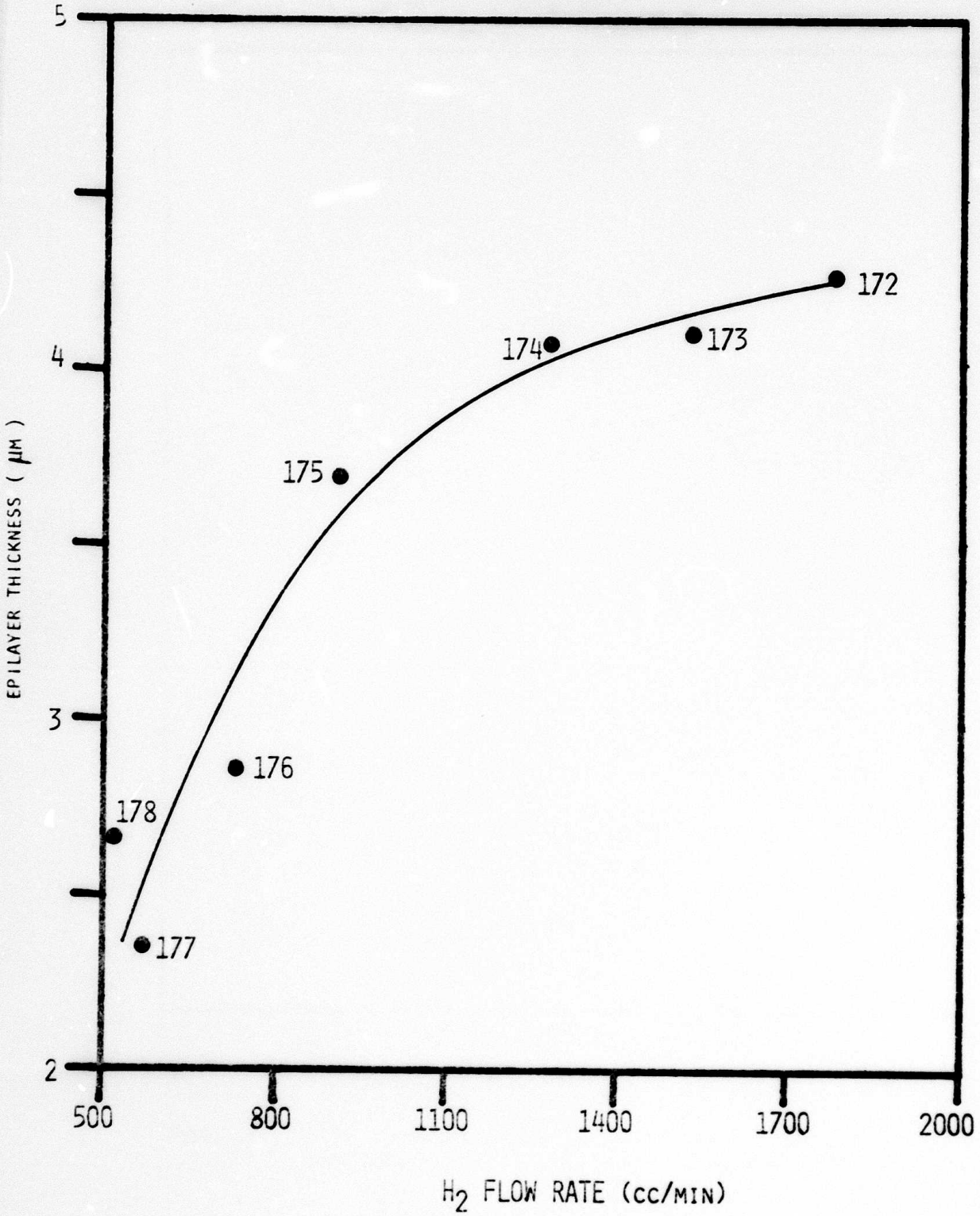

Fig. 2.3 The epitaxial layer thickness versus the H_2 flow rate for samples 172 through 178.

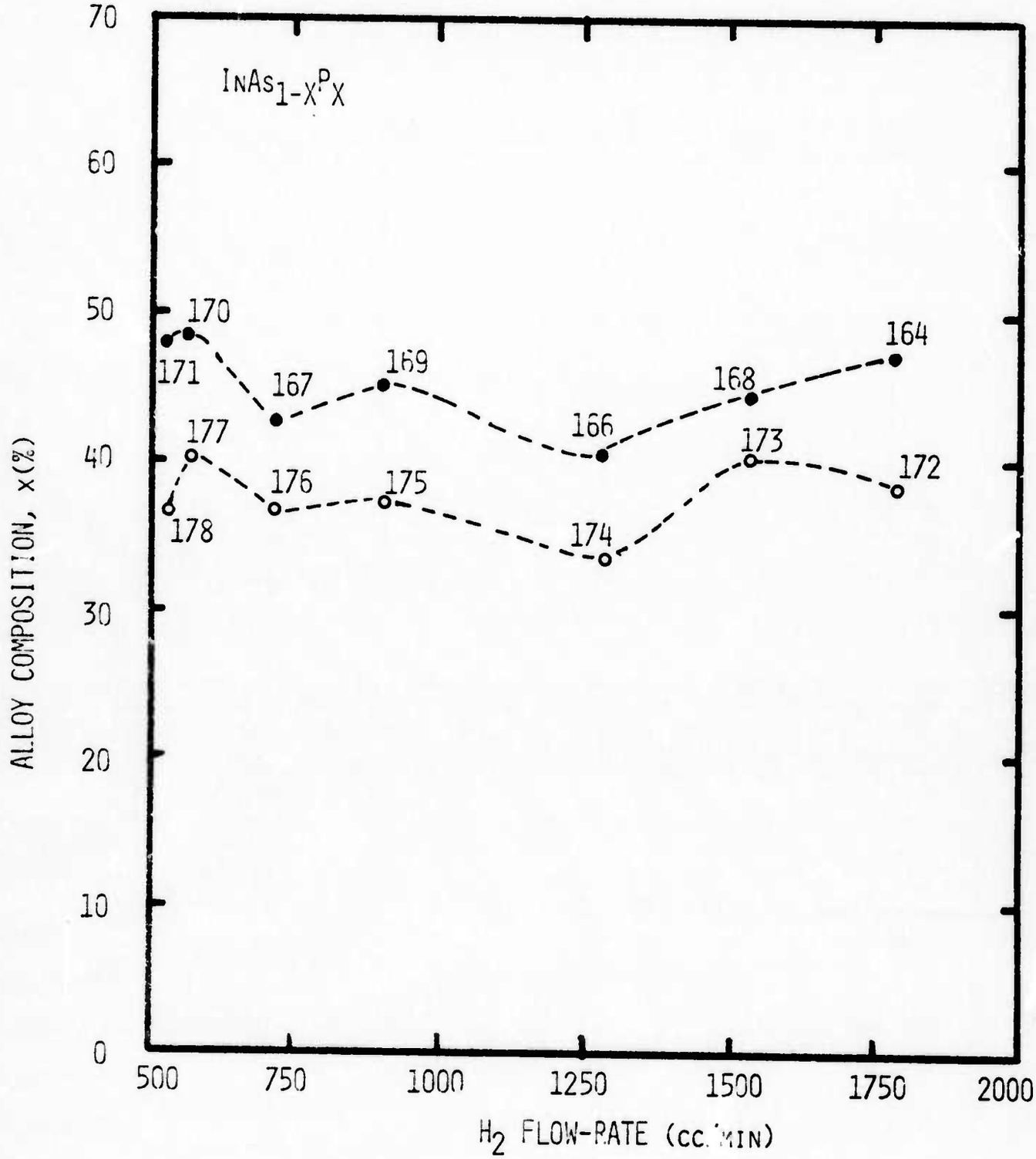

Fig. 2.4 Alloy composition (%) versus hydrogen carrier gas flow rate for fourteen $InAs_{1-x}P_x$ epitaxial specimens (164-178).

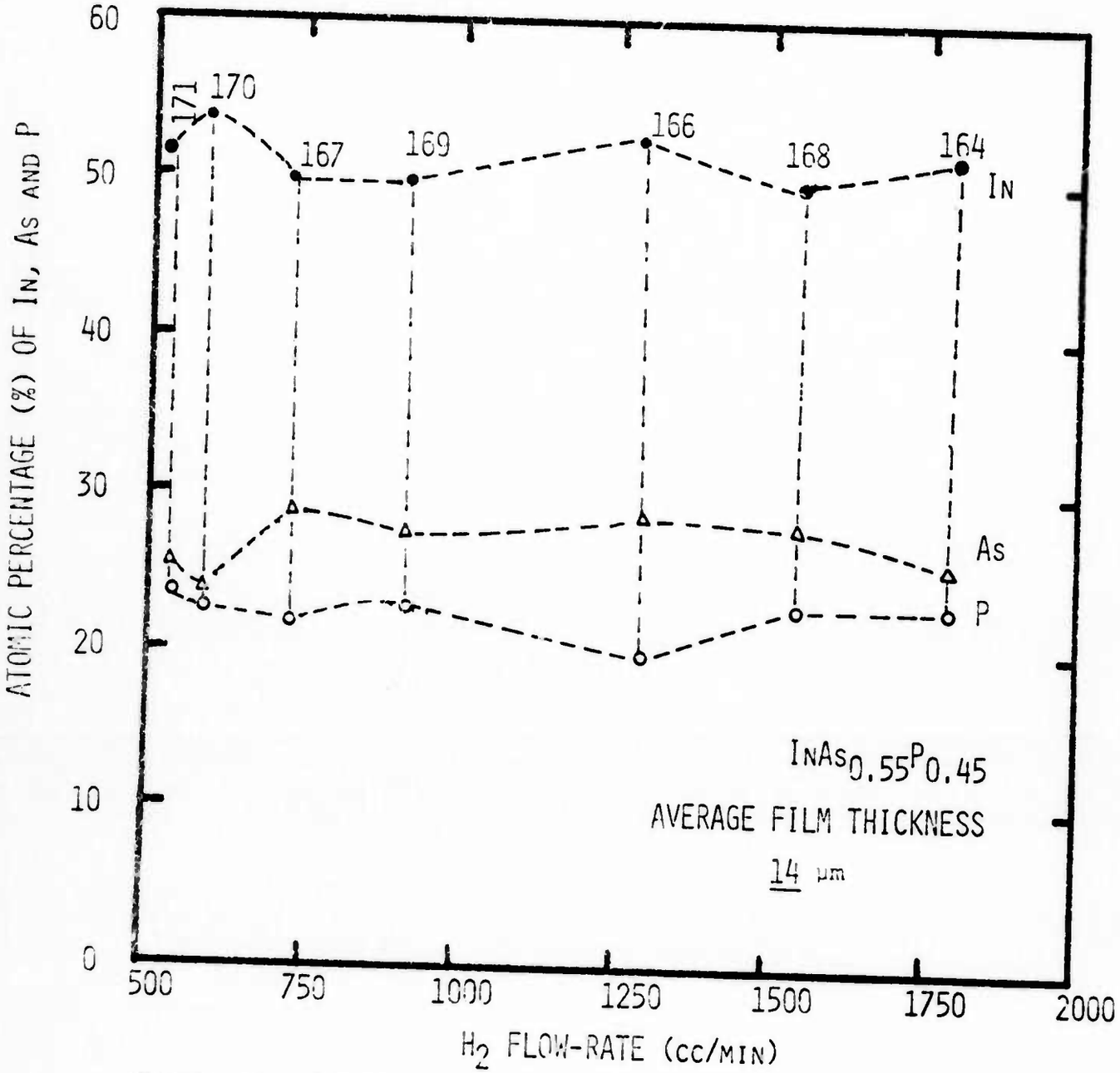

Figure 2.5 The atomic composition (%) of In, As and P versus the hydrogen carrier gas glow rate for seven $InAs_{1-x}P_x$ epitaxial samples (164-171).

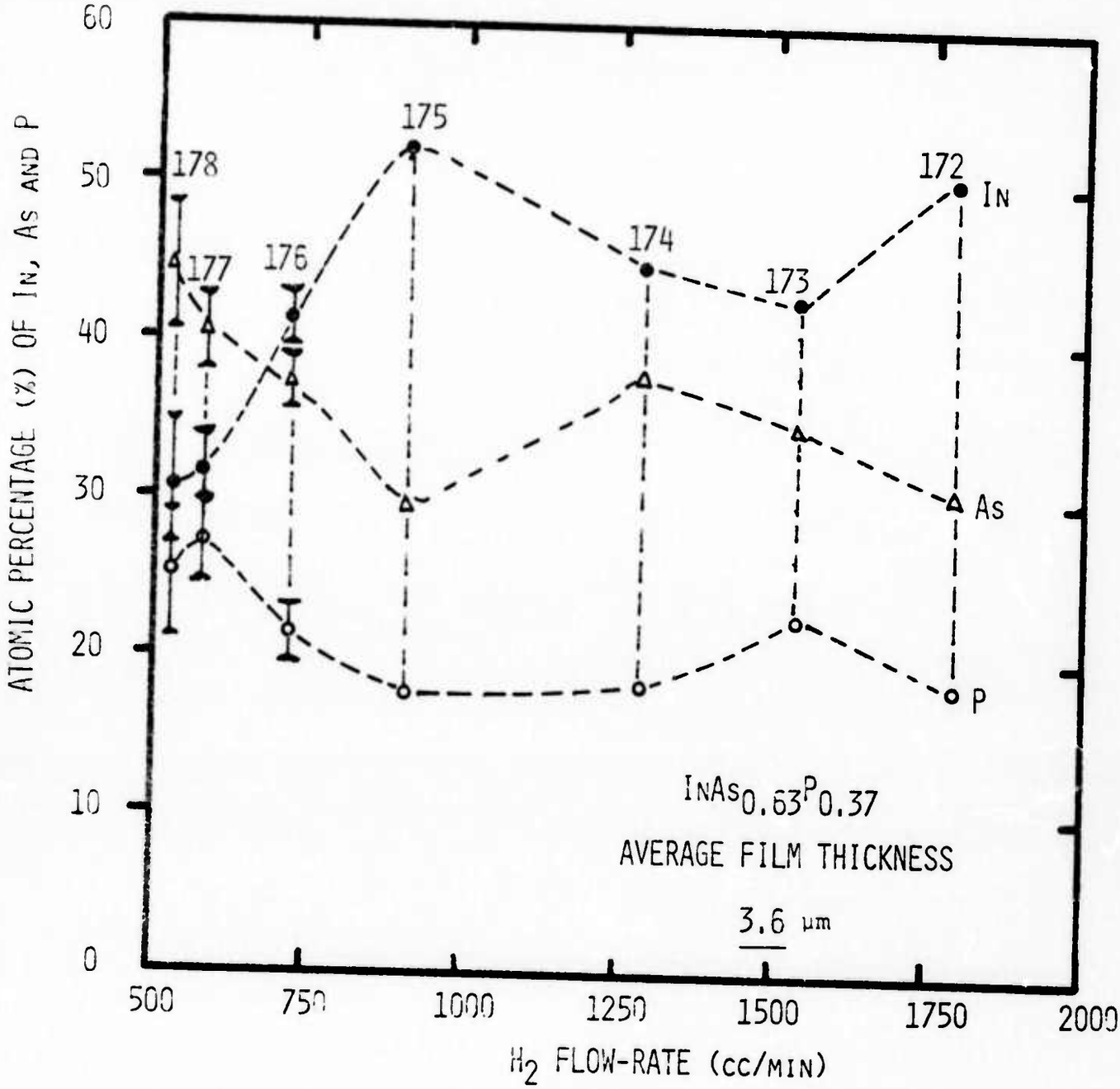

Fig. 2.6 The atomic composition of In, As and P versus the hydrogen carrier gas flow rate for seven $InAs_{1-x}P_x$ samples (172-178).

III. TRANSPORT PROPERTIES OF $InAs_{0.63}P_{0.37}$ EPITAXIAL SAMPLES

In this chapter, experimental results on the transport properties of seven $InAs_{0.63}P_{0.37}$ epitaxial samples (samples 172-178) are presented. The experimental tools employed include resistivity, the Hall effect, and magnetoresistance measurements. Transport coefficients, such as resistivity, Hall coefficient, electron concentration and mobility, and transverse magnetoresistance coefficient as functions of temperature ($4.2°K < T < 300°K$), are deduced from these measurements.

3.1 Resistivity and Hall Coefficient Data

Resistivity and Hall effect measurements have been performed for epitaxially grown $InAs_{0.63}P_{0.37}$ samples 172, 174 and 176, at temperatures between 4.2°K and 300°K, and for samples 175, 173, 177 and 178 at temperatures between 77°K and 300°K. The thickness of these epitaxial samples as a function of the H_2 flow rate was shown in Fig. 2.3. Note that the growth conditions for this set of samples were identical to those of samples 164-171 reported previously[1], with the exception of the deposition time (which was reduced to six minutes for this set of samples). As a result, the film thicknesses varied from 2.35 μm to 4.3 μm, as the H_2 flow-rate changed from 515 cc/min. to 1780 cc/min. The film quality for this set of samples can be classified from good to poor. As will be discussed later, sample 175 showed highest electron mobility, and samples 177 and 178 (2 μm films) showed very low electron mobility and highly nonstochiometric structures.

Fig. 3.1 shows the resistivity versus inverse absolute temperature for samples 172 (H_2 flow rate 1780 cc/min.), 174 (1280 cc/min.), and 176 (730 cc/min.), for temperatures between 4.2°K and 300°K. The results show that the resistivity increases with a decreasing H_2 flow rate. The resistivity increases exponentially with inverse temperature for 20°K < T < 300°K, and then increases linearly with decreasing temperature for T < 20°K. These results are consistent with the previously observed and reported results for samples 164-171[1]. From Fig. 3.1, it is noted that for temperatures between 20°K and 300°K, the conductivity versus temperature curves can be represented by Eq. (3.1):

$$\sigma(T) = C_1 \exp(-E_1/kT) \quad , \quad \text{for} \quad 20°K < T < 300°K \tag{3.1}$$

where E_1 is the conductivity activation energy and C_1 is a constant, independent of temperature. Values of E_1 were calculated for three samples from Fig. 3.1. The results are listed in Table 3.1.

For temperatures below 20°K, the impurity hopping conduction dominates. The resistivity was found to increase linearly with decreasing temperature, as is shown in Fig. 3.2, 3.3 and 3.4 for samples 172, 174 and 176 respectively. This is also consistent with our previous observation for samples 164 through 171[1]. Fig. 3.5 shows the resistivity versus inverse absolute temperature plot for samples 173, 175, 177 and 178, for temperatures between 77°K and 300°K. With the exception of sample 173, the resistivity for T > 100°K was found to increase with an increasing H_2 flow-rate, while for sample 173, a minimum value of resistivity was observed at 130°K.

To illustrate the dependence of the resistivity on the hydrogen carrier gas flow rate, Fig. 3.6 shows a plot of resistivity versus the H_2 flow rate for samples 172 through 178, at T = 300°K and T = 77°K. The results indicate that a maximum resistivity occurs as the H_2 flow rate varies from 515 cc/min to 1780 cc/min. The peak value appears to shift towards the lower H_2 flow rate end as the temperature is decreased.

The Hall coefficient versus the inverse absolute temperature for samples 172, 174 and 176 is displayed in Fig. 3.7. The results show that the Hall coefficient increases exponentially with decreasing temperatures for T < 300°K, and passes a peak value between 50°K and 100°K; it then decreases exponentially with decreasing temperature and finally reaches a constant plateau for T < 10°K. This result is consistent with results we had previously observed for samples 153-159 and 164-171[1-2]. Note that the peak Hall coefficient for these three curves shifts toward the lower temperature end as the H_2 flow rate is increased. The temperature dependence of the Hall coefficient for samples 173, 175, 177 and 178 shown in Fig. 3.8 is similar to that of samples 172, 174 and 176, shown in Fig. 3.7. The peak value of the Hall coefficient for these samples also shifts toward the lower temperature end as the H_2 flow rate is increased. This similar phenomena has also been observed in compensated germanium samples[3].

The dependence of the Hall coefficient on the magnetic field is shown in Fig. 3.9 for samples 172 through 178, for T = 77°K. The results show that the Hall coefficient for these

samples depends very weakly on the magnetic field; sample 175, however, does show a stronger dependence on the magnetic field.

3.2 Electron Mobility

The Hall mobility was calculated from the resistivity and the Hall coefficient data displayed in Fig. 3.1, 3.2, 3.7 and 3.8, using the relation

$$\mu_H = \sigma R_H \quad . \tag{3.2}$$

Fig. 3.10 shows the Hall (electron) mobility versus the inverse absolute temperature plot for samples 172, 174 and 176, for temperatures between 4.2°K and 300°K. The maximum electron mobility was 3850 cm^2/V-s for sample 176, 4900 cm^2/V-s for sample 174, and 6600 cm^2/V-s for sample 172. The electron mobility increased with increasing flow rate for these three samples (see Fig. 3.12). The Hall mobility versus the reciprocal temperature for samples 175, 173, 177 and 178 is shown in Fig. 3.11. The results show that samples 175 and 173 had a relatively high electron mobility, while samples 177 and 178 had a rather low electron mobility compared to the other samples measured (samples 172-176). This result could be attributed to the fact that these two samples have the thinnest epitaxial layer (~2 μm) among this set, and that the nonstochiometric structures, lattice mismatching and other imperfections at the interfacial layer could have a drastic effect on the electron mobility.

The results show that room temperature electron mobility varies from about 2800 cm^2/V-s for samples 178 and 177, to

5000 cm^2/V-s for sample 173. A plot of the electron mobility as a function of the H_2 carrier gas flow rate for T = 4.2°K, 77°K and 300°K is illustrated in Fig. 3.12, which shows that the electron mobility increases with an increasing H_2 flow rate. However, it was also found that the electron mobility for this set of samples is generally lower than for samples 164-171 reported previously[1], implying that the film quality for this set of samples may not be as good as for samples 164-171. The main reason for this reduction in electron mobility may be the fact that the film thicknesses for this set of samples are all less than 5 μm, and that the effects of the lattice mismatching and nonstochiometric structure, and imperfections at the interface between substrate and the epilayer all play an important role in limiting electron mobility.

3.3 Electron Concentration

The electron concentration can be calculated from the Hall coefficient data using the relationship

$$n = \frac{\gamma}{q R_H} \quad , \tag{3.3}$$

where γ is the scattering factor varying between 1 and 2, depending upon the types of scattering processes involved.

From the results of the Hall coefficient versus magnetic field curves, shown in Fig. 3.9, we assumed that $\gamma = 1$ and calculated the electron concentration, n, from Eq. (3.2), for samples 172 through 178. The results are shown in Fig. 3.13 and 3.14. The electron concentration at 77°K was found to vary from 7 x 10^{15} cm^{-3} for sample 175 to 4.3 x 10^{16} cm^{-3} for

sample 178, while the room temperature electron concentration varied from 2.4×10^{16} cm^{-3} for sample 175 to 6×10^{16} cm^{-3} for sample 178.

To illustrate the effect of the hydrogen carrier gas flow rate on the electron concentration of samples 172 through 178, Fig. 3.15 displays such a plot for T = 4.2°K, 77°K and 300°K. The results for T = 4.2°K indicated that the electron concentration decreases with an increasing H_2 flow rate. However, the results for T = 77°K and 300°K are rather scattered and inconclusive. It appears that there is an optimum H_2 flow rate, which would yield a minimum electron concentration in these samples.

3.4 Magnetoresistance Data

Transverse magnetoresistance measurements have been made for samples 173 through 178 at T = 77°K, and for samples 172, 174 and 176 at T = 4.2°K. The results are plotted in Fig. 3.16 and Fig. 3.17, respectively. Fig. 3.16 shows the $\Delta\rho/\rho_o$ versus B^2 for samples 173 through 178, for T = 77°K. The results show that the magnetoresistance data are positive and $\Delta\rho/\rho_o$ is proportional to B^2. This result led us to the conclusion that the conduction band structure for these InAsP samples is parabolic. The magnetoresistance at low magnetic field (i.e., $\mu B << 1$) can be written as

$$\frac{\Delta\rho}{\rho_o} = \mu_H^2 B^2 \left[\frac{\langle\tau^3\rangle\langle\tau\rangle}{\langle\tau^2\rangle^2} - 1\right]$$

$$= \zeta\mu_H^2 B^2 \quad , \tag{3.4}$$

where

$$\zeta = \left[\frac{\langle\tau^3\rangle\langle\tau\rangle}{\langle\tau^2\rangle^2} - 1\right]$$

is defined as the magnetoresistance coefficient. $\zeta = 0.57$ for ionized impurity scattering, and $\zeta = 0.275$ for acoustical phonon scattering.

To compare the experimental results shown in Fig. 3.16 with the value predicted by Eq. (3.4), we substitute the Hall mobility data for samples 175 and 173 into Eq. (3.4), and compute the magnetoresistance coefficient ζ. The results are $\zeta = 0.514$ for sample 175, and 0.444 for sample 173. These values compare favorably with the theoretical value of $\zeta = 0.57$ for ionized impurity scattering. The result indicates that ionized impurity scattering is indeed dominant at T=77°K for these two samples. The magnetoresistance data at T = 4.2°K for samples 172, 174 and 176 are all negative. (See Fig. 3.17.) This is attributed to the impurity band conduction described in our previous report[1].

3.5 Concluding Remarks on the Conduction Processes in InAsP Epitaxial Samples

Our studies on the conduction processes in InAsP alloy systems have led us to the conclusion that the electrical conductivity in these specimens can, in general, be expressed by

$$\sigma(T) = C_1 \exp(-E_1/kT) + C_2(T) \quad . \tag{3.5}$$

E_1 is the familiar donor ionization energy and is generally observed in the higher temperature range for InAsP samples studied.

It is seen to increase with decreasing donor concentration as illustrated by samples 172, 174, and 176. The activation energy E_1 generally increases monotonically with compensation, as has been reported in a germanium specimen[3]. C_1 is the extrapolated value of $\sigma(T)$ for $1/T \to 0$.

The second term, $C_2(T)$, of equation 3.5 represents the low temperature conductivity which showed a slight linear increase with increasing temperature. In this temperature region, conduction in samples of low impurity concentration is normally attributed to hopping of electrons from occupied to unoccupied localized impurity states[4]. An activation energy E_3 is associated with this hopping transition[5-7]. However, at higher concentrations the impurity states overlap and lose their localized nature forming an impurity band. Davis and Compton[3] have shown that E_3 disappears in germanium samples upon formation of this band. This seems to be indicative of the results shown for the three samples 172, 174 and 176. The small temperature dependence might be attributed to a slight localization of the donor states or to small compensation effects. It appears that hopping type conduction is not a dominant process in these specimens. Our ac conductivity measurements* support this argument.

As for the temperature dependence of the Hall coefficient (for samples with intermediate doping range), the Hall coefficient passes through a single maximum value near the

---

*Our measurements on frequency dependence of ac conductivity in InAsP epitaxial samples so far show very little change in ac conductivity with frequency. This indicates that the polarization effect due to hopping conduction is very small in these samples.

temperature at which the conduction via the impurity levels equals that in the conduction band. This is clearly observed in most of our InAsP specimens[1-2].

In summary, the impurity conduction in InAsP samples is observed at temperatures sufficiently low enough that most electrons are frozen out of the conduction band. The resistivity-temperature curves exhibit activation energies which are functions both of the donor concentration and of the compensation. The Hall coefficient passes through a maxima as the temperature decreases.

The magnetoresistance coefficients are positive for $T > 20°K$, and show a linear dependence on the square of the magnetic flux density. However, for $T < 20°K$, the negative magnetoresistance results, implying the beginning of the dominant impurity conduction process taking place in these specimens.

TABLE 3.1 Conductivity Activation Energy, E_1, for three $InAs_{0.63}P_{0.37}$ epitaxial samples observed for $20°K < T < 300°K$.

Sample No.	172	174	176
H_2-Flow Rate (cc/min.)	1780	1280	730
E_1 (meV)	1.71	3.11	5.31

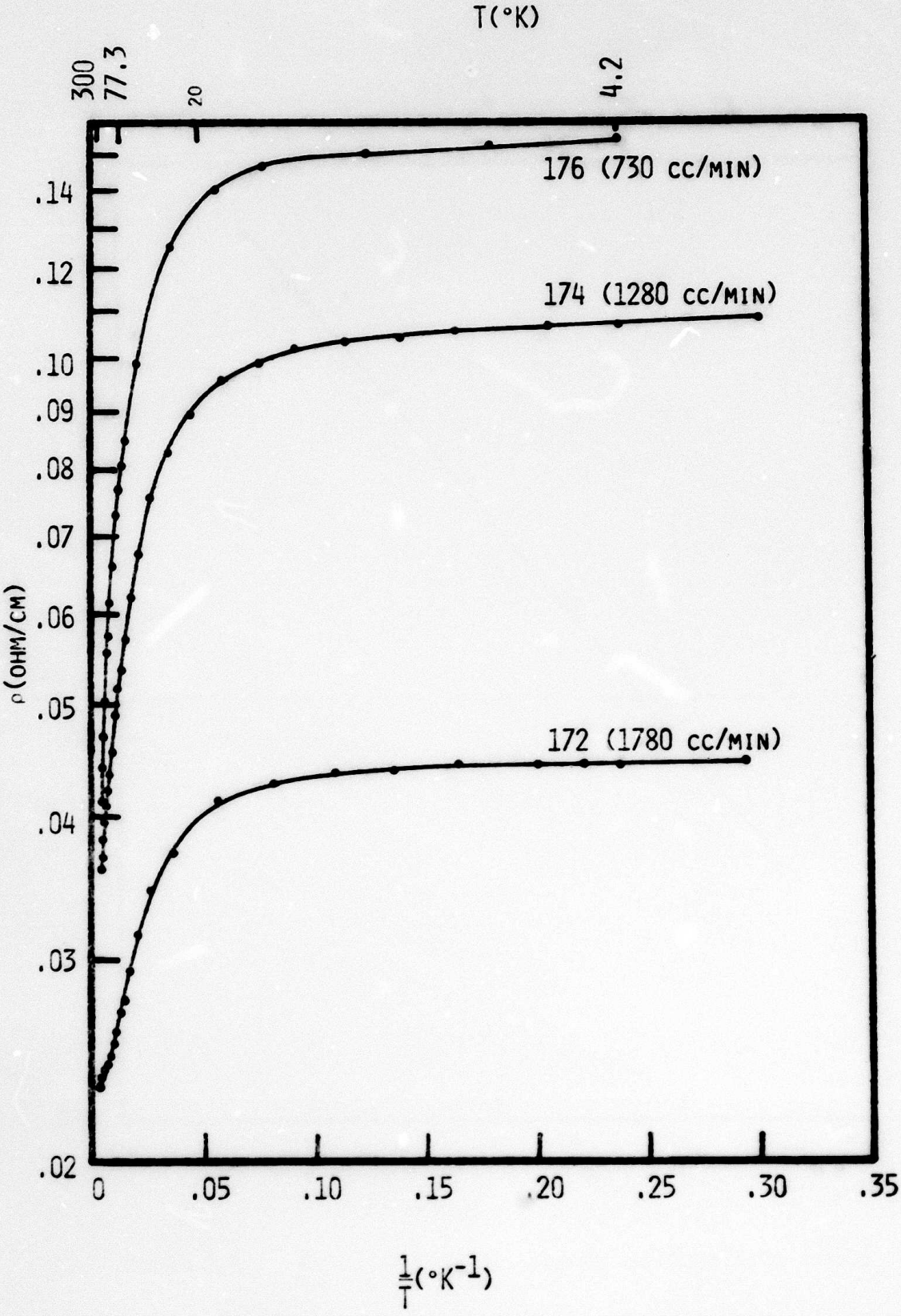

Fig. 3.1 The electrical resistivity versus the reciprocal temperature for $InAs_{0.63}P_{0.37}$ epitaxial samples 172, 174 and 176, for $4.2°K < T < 300°K$.

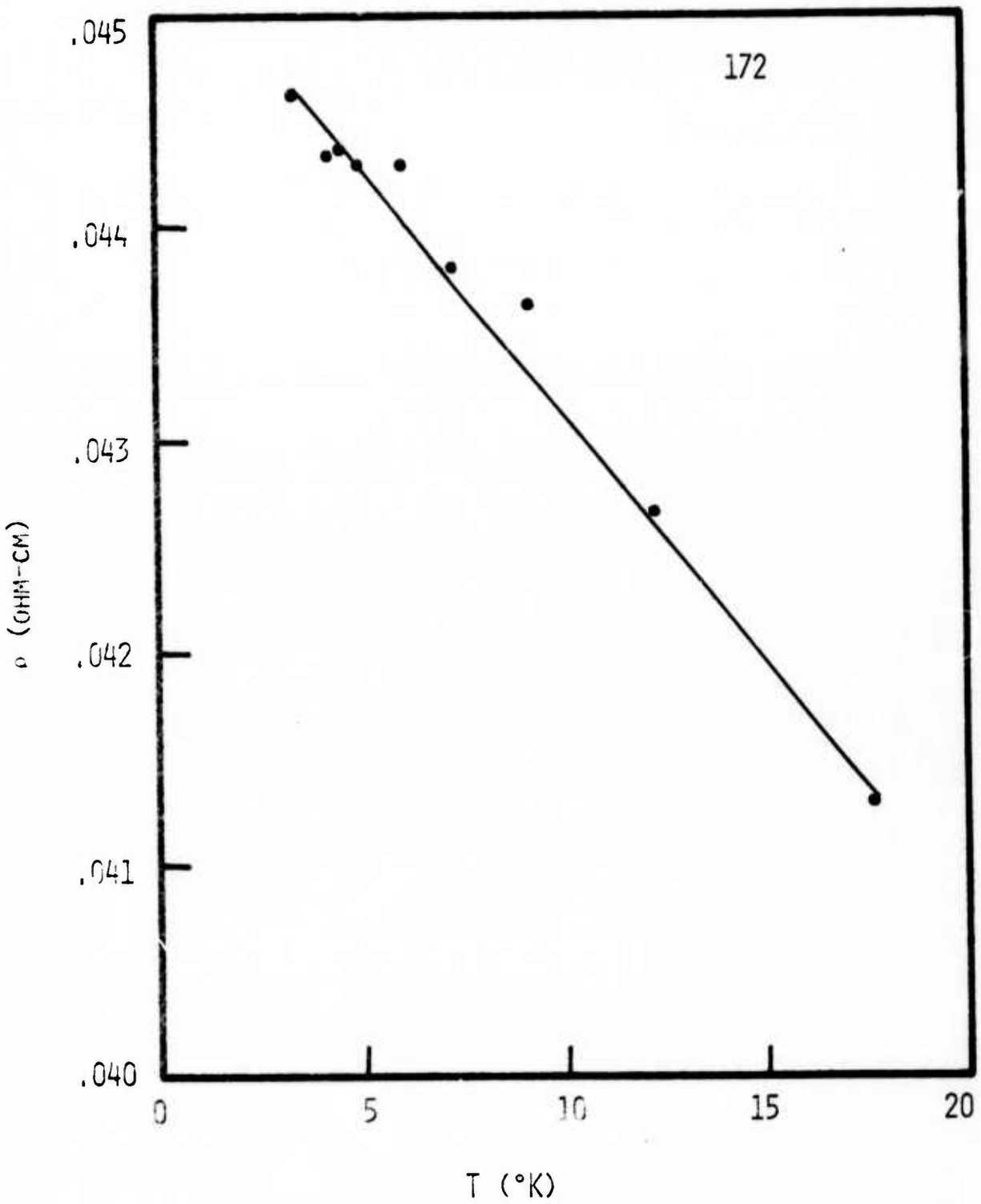

Figure 3.2 Resistivity versus absolute temperature for sample 172 for T < 20°K.

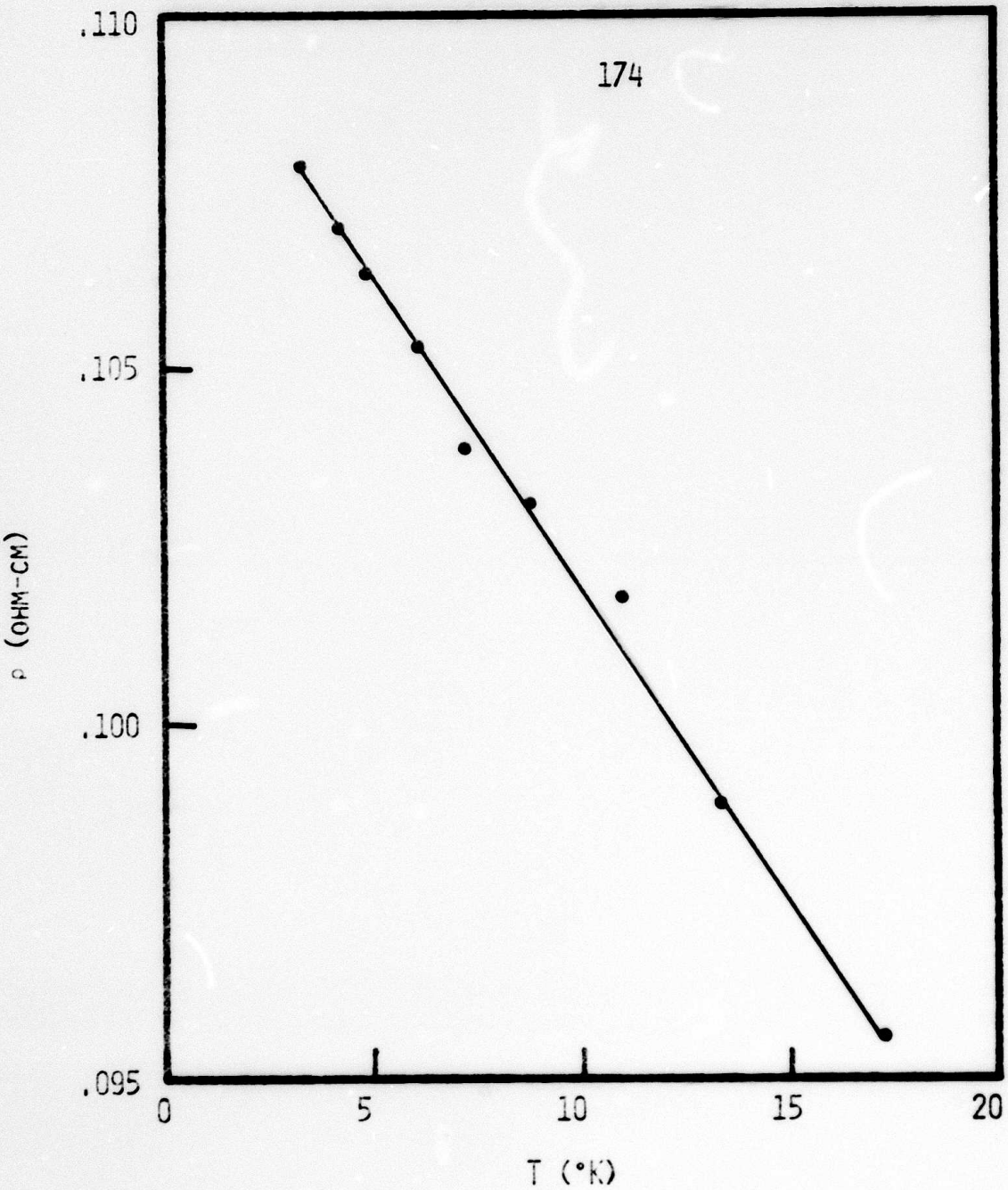

Figure 3.3 Resistivity versus absolute temperature for sample 174 for T < 20°K.

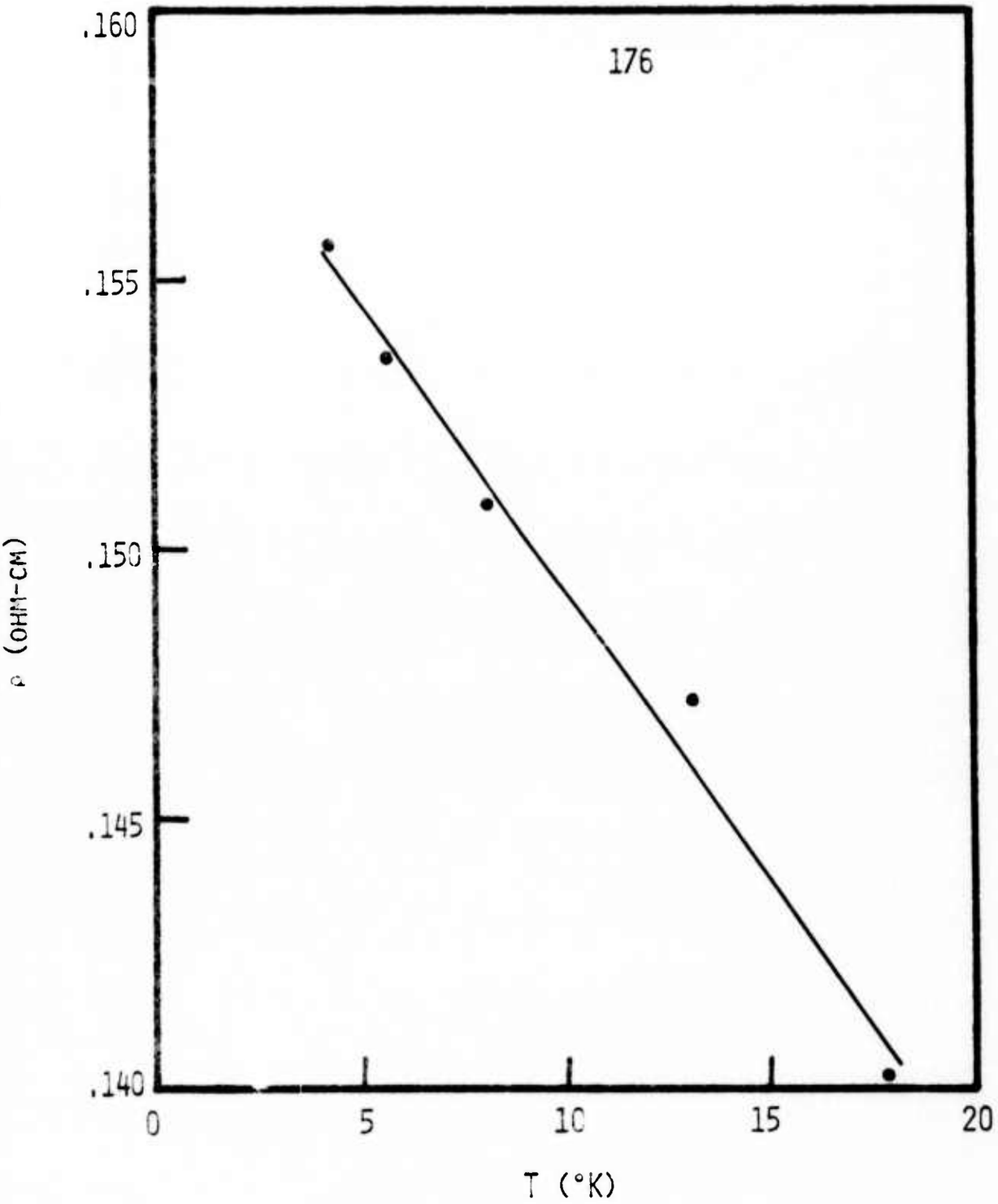

Figure 3.4 Resistivity versus absolute temperature for sample 176 for T < 20°K.

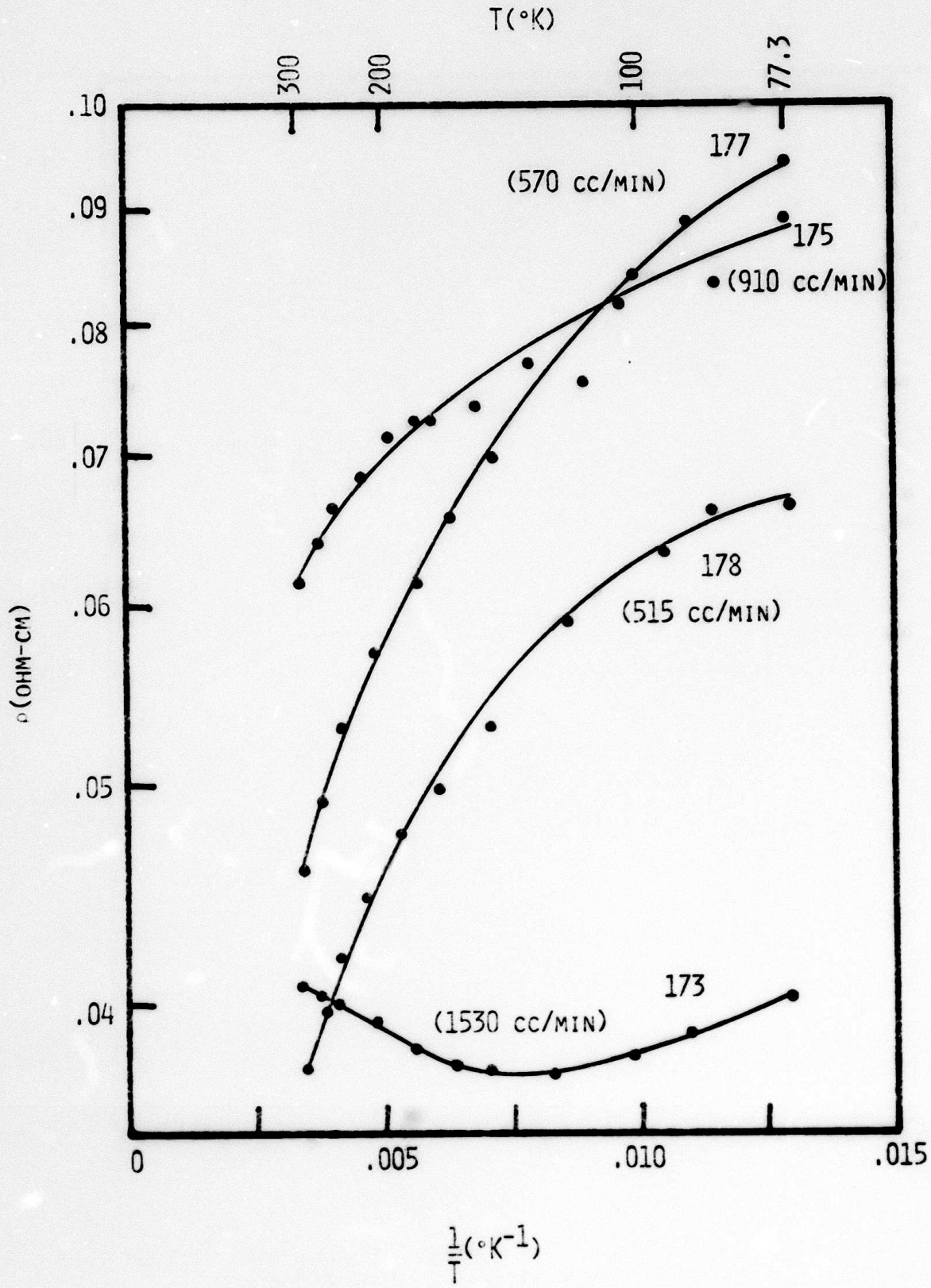

Fig. 3.5 The electrical resistivity versus the reciprocal temperature for $InAs_{0.63}P_{0.37}$ epitaxial samples 173, 175, 177 and 178, for $77°K < T < 300°K$.

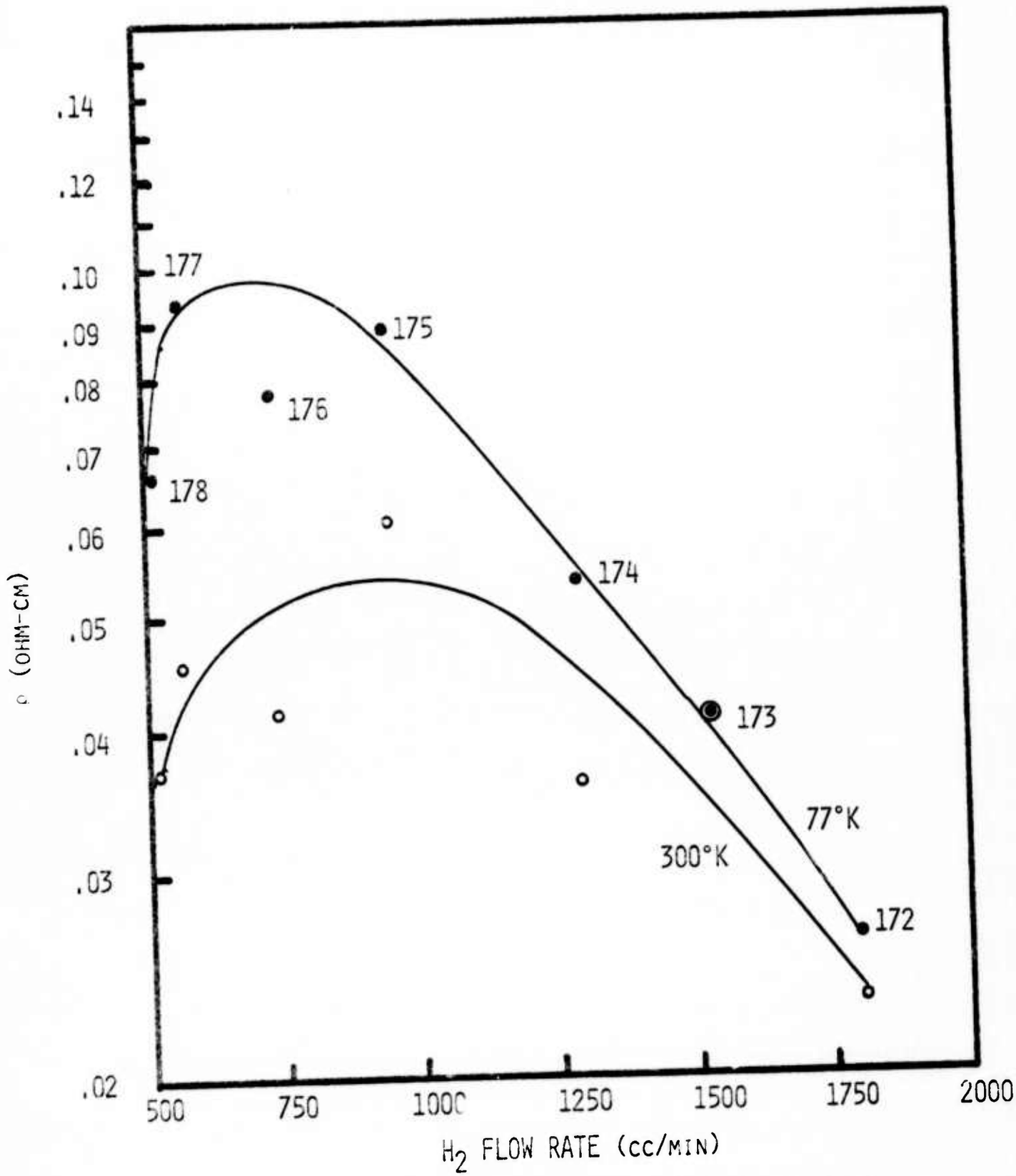

Fig. 3.6 The electrical resistivity versus tne hydrogen carrier gas flow rate T = 77°K and 300°K.

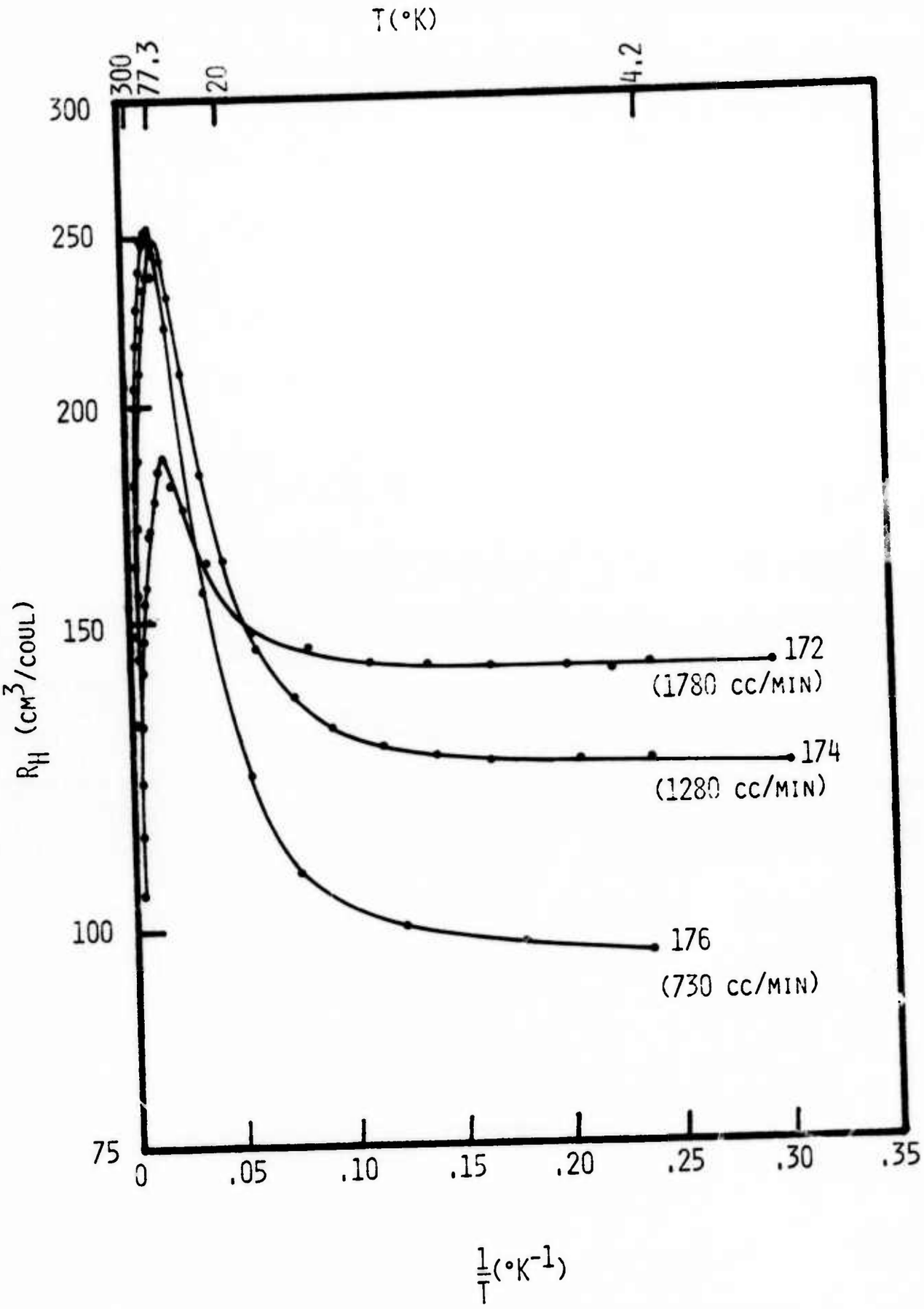

Fig. 3.7 The Hall coefficient versus the reciprocal temperature for samples 172, 174 and 176, for 4.2°K < T < 300°K

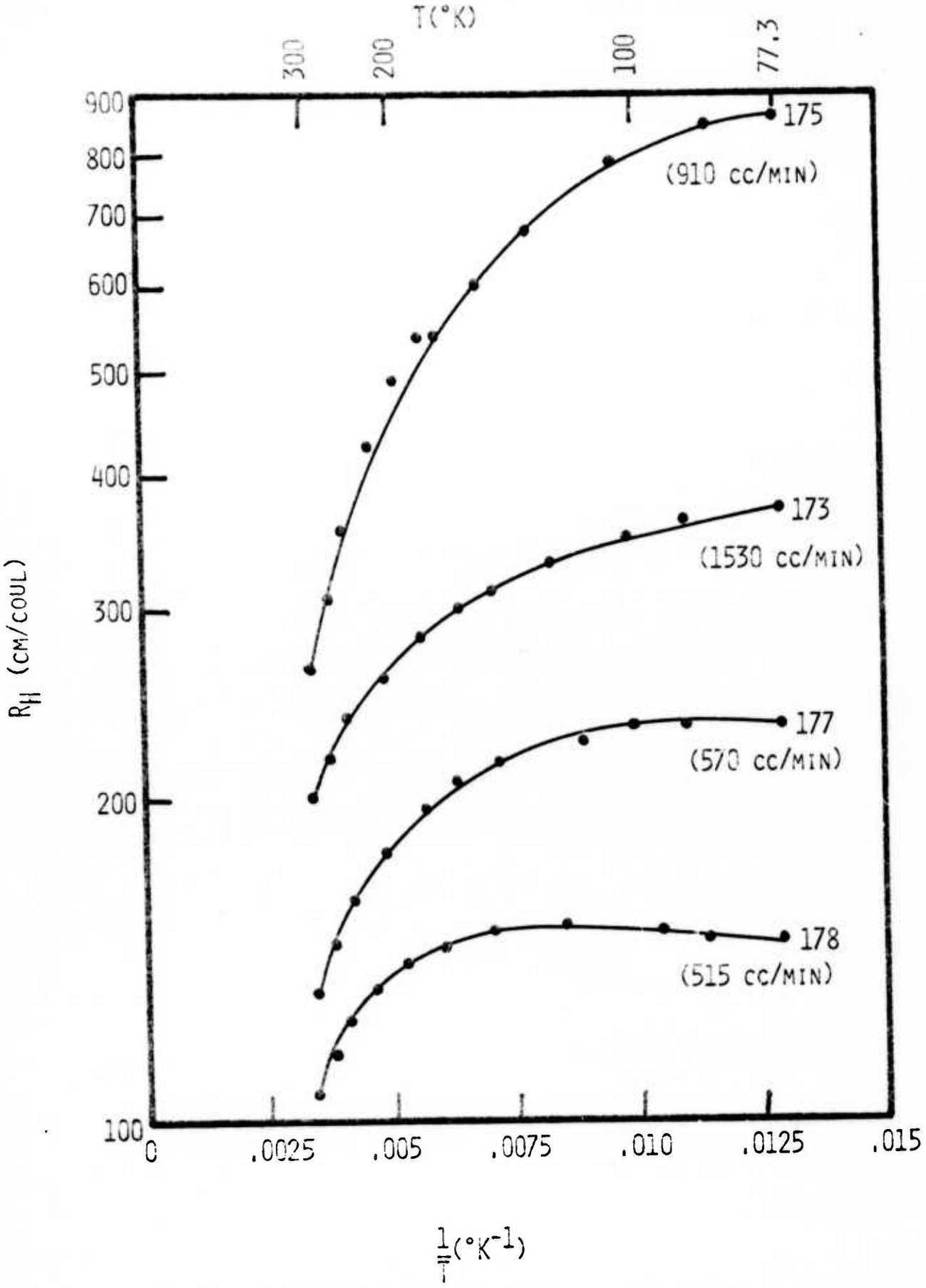

Fig. 3.8 The Hall coefficient versus the reciprocal temperature for samples 173, 175, 177 and 178, for 77°K < T < 300°K.

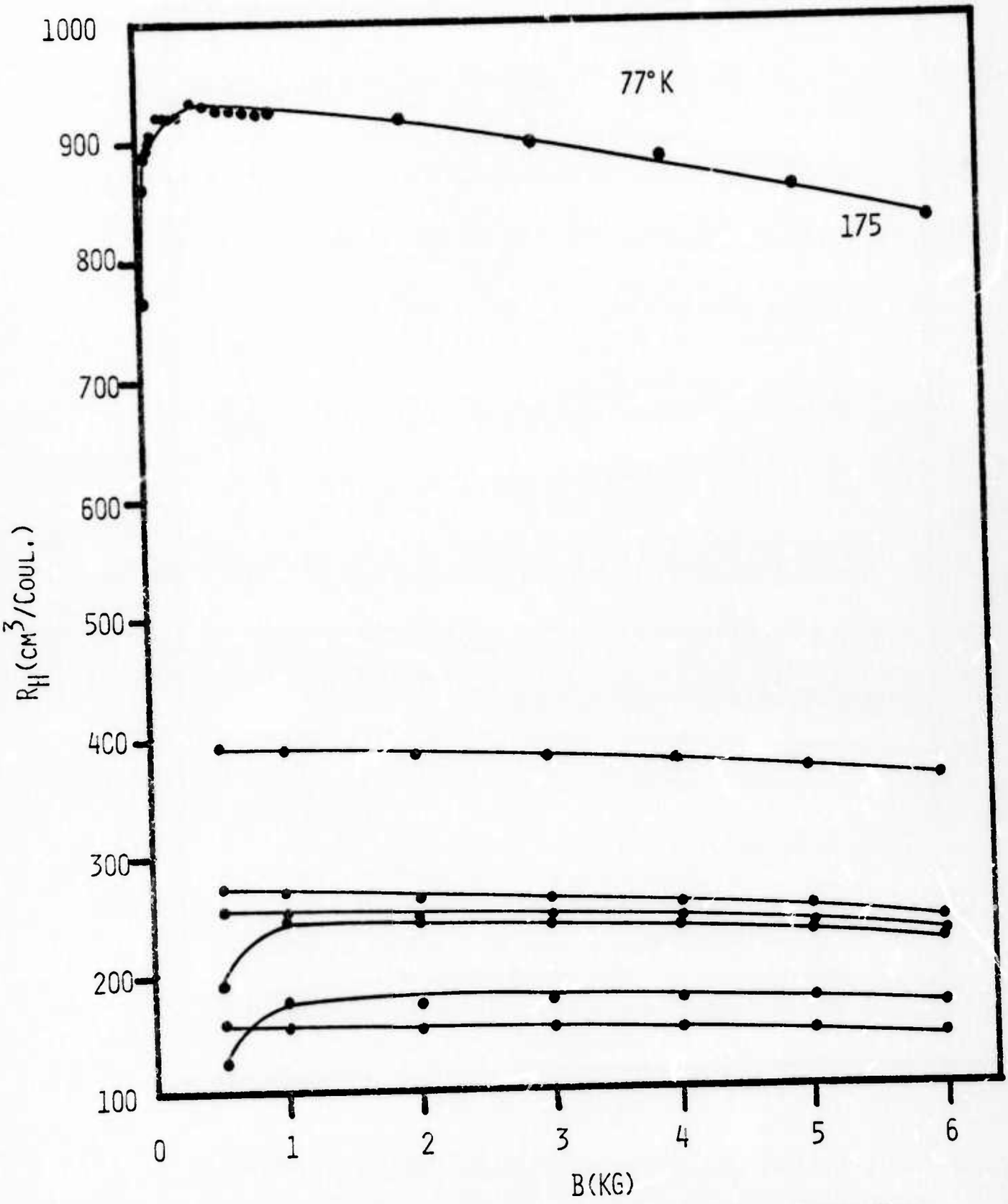

Fig. 3.9 The Hall coefficient as a function of the magnetic flux density for samples 172-178 at T = 77°K.

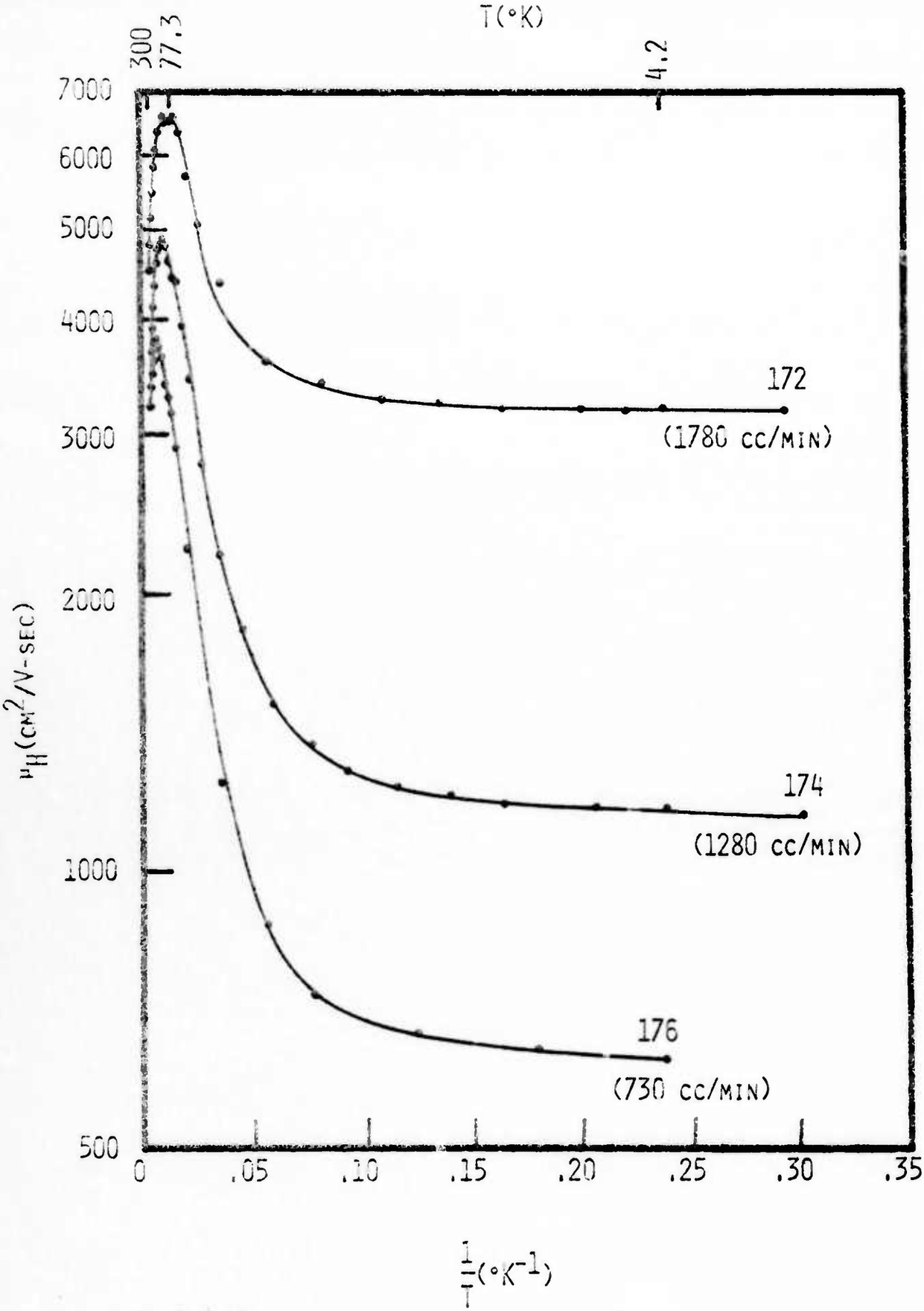

Fig. 3.10 The electron mobility versus the reciprocal temperature for samples 172, 174 and 176 for $4.2°K < T < 300°K$. Note that the maximum mobility point in each curve shifts towards the lower temperature side as the H_2 flow rate is increased.

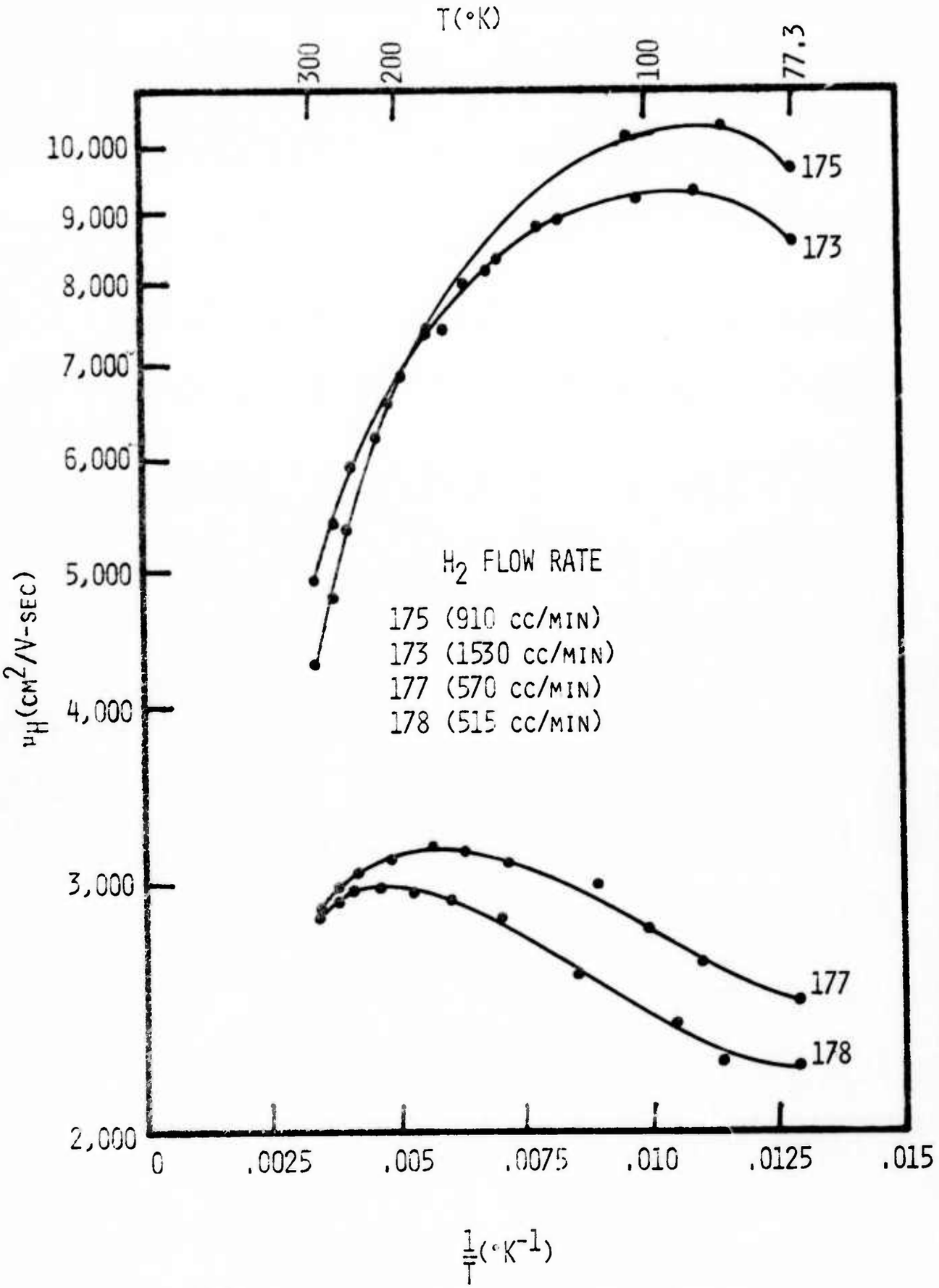

Fig. 3.11 The electron mobility versus the reciprocal temperature for samples 173, 175, 177 and 178, for 77°K < T < 300°K.

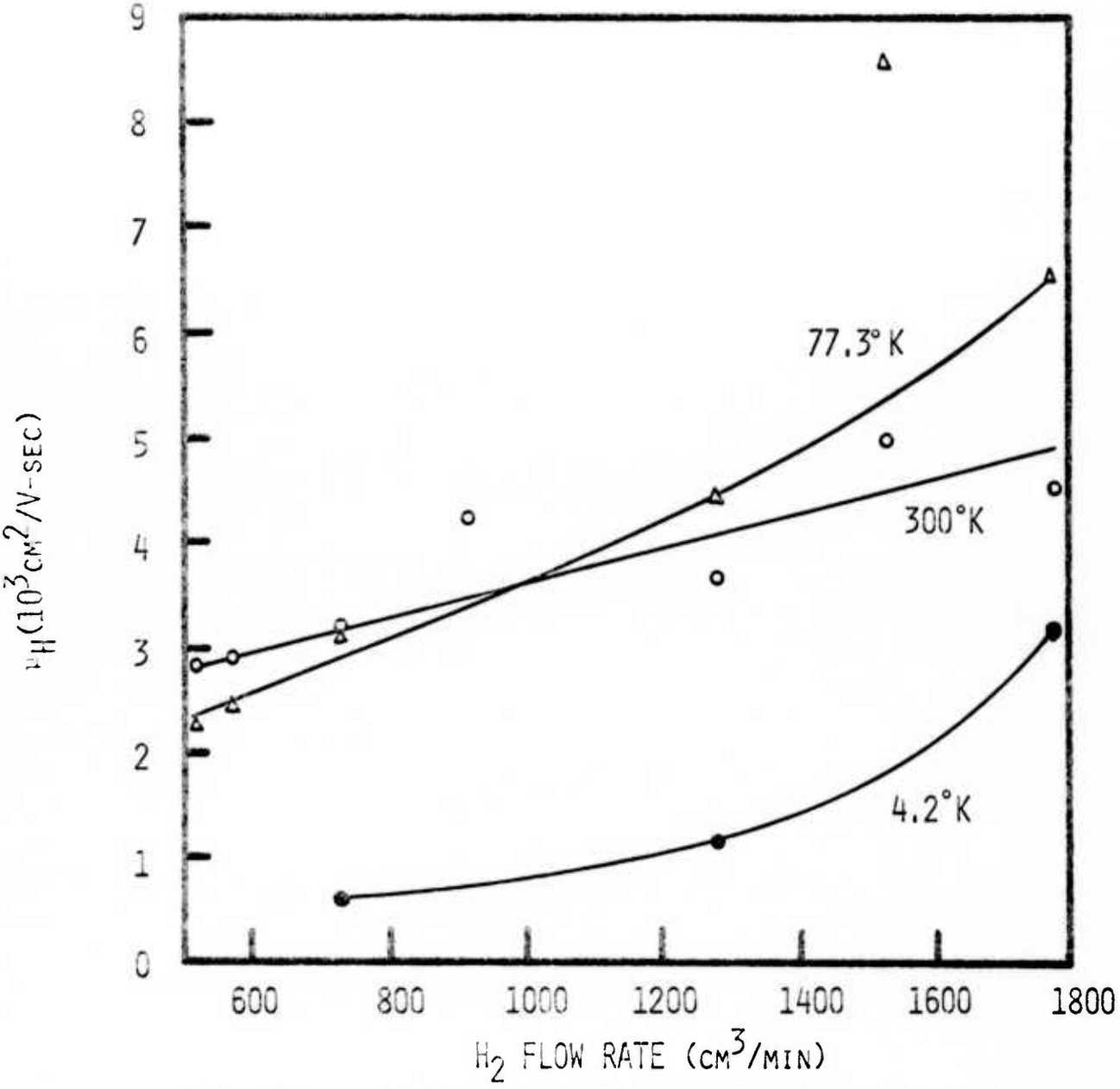

Fig. 3.12 The electron mobility as a function of the H_2 flow rate for samples 172-178, at T = 4.2°K, 77 °K and 300°K. The electron mobility appears to increase with H_2 flow rate for this set of samples.

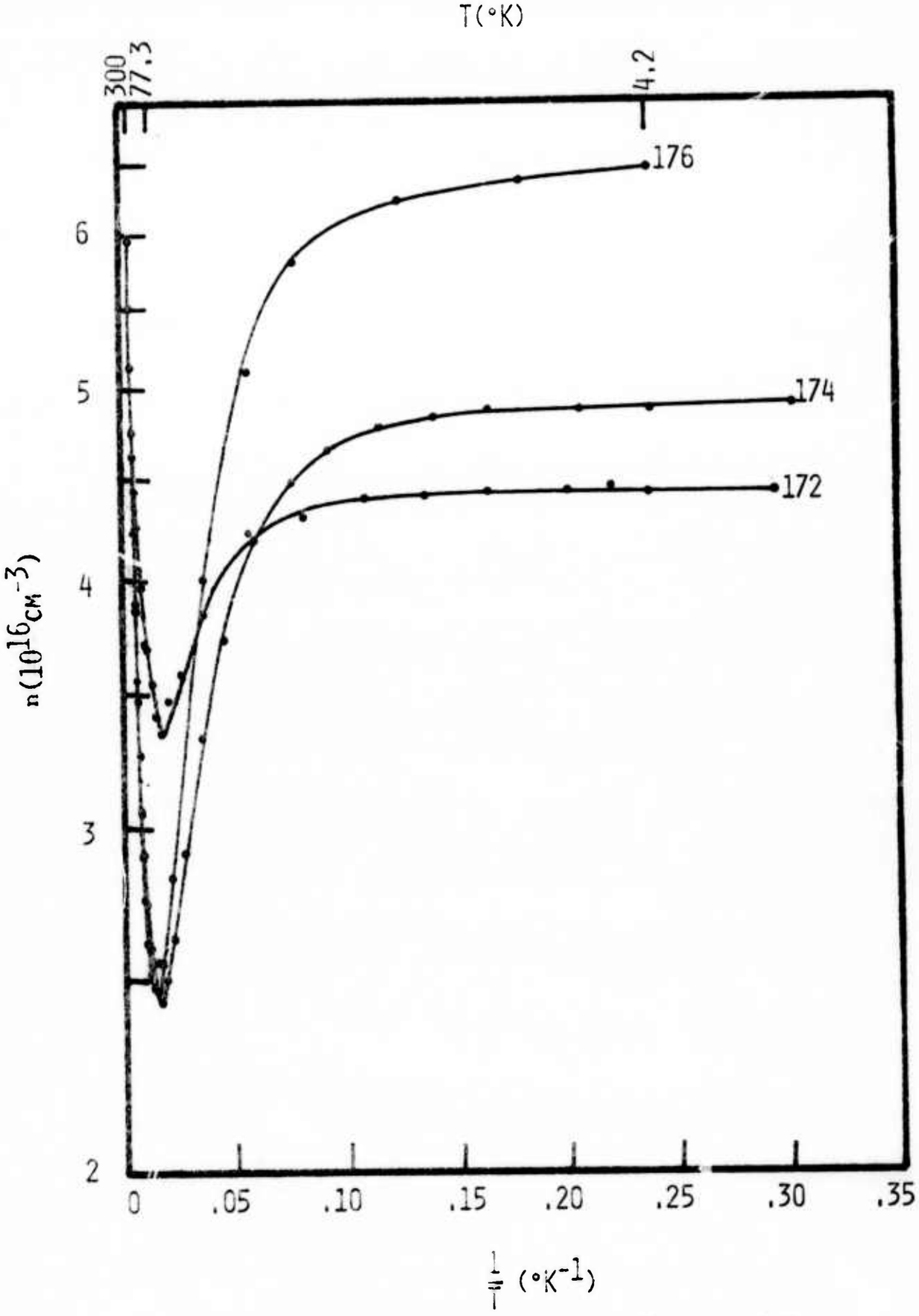

Fig. 3.13 The electron concentration as a function of the reciprocal temperature for samples 172, 174 and 176, for temperatures between 4.2°K and 300°K.

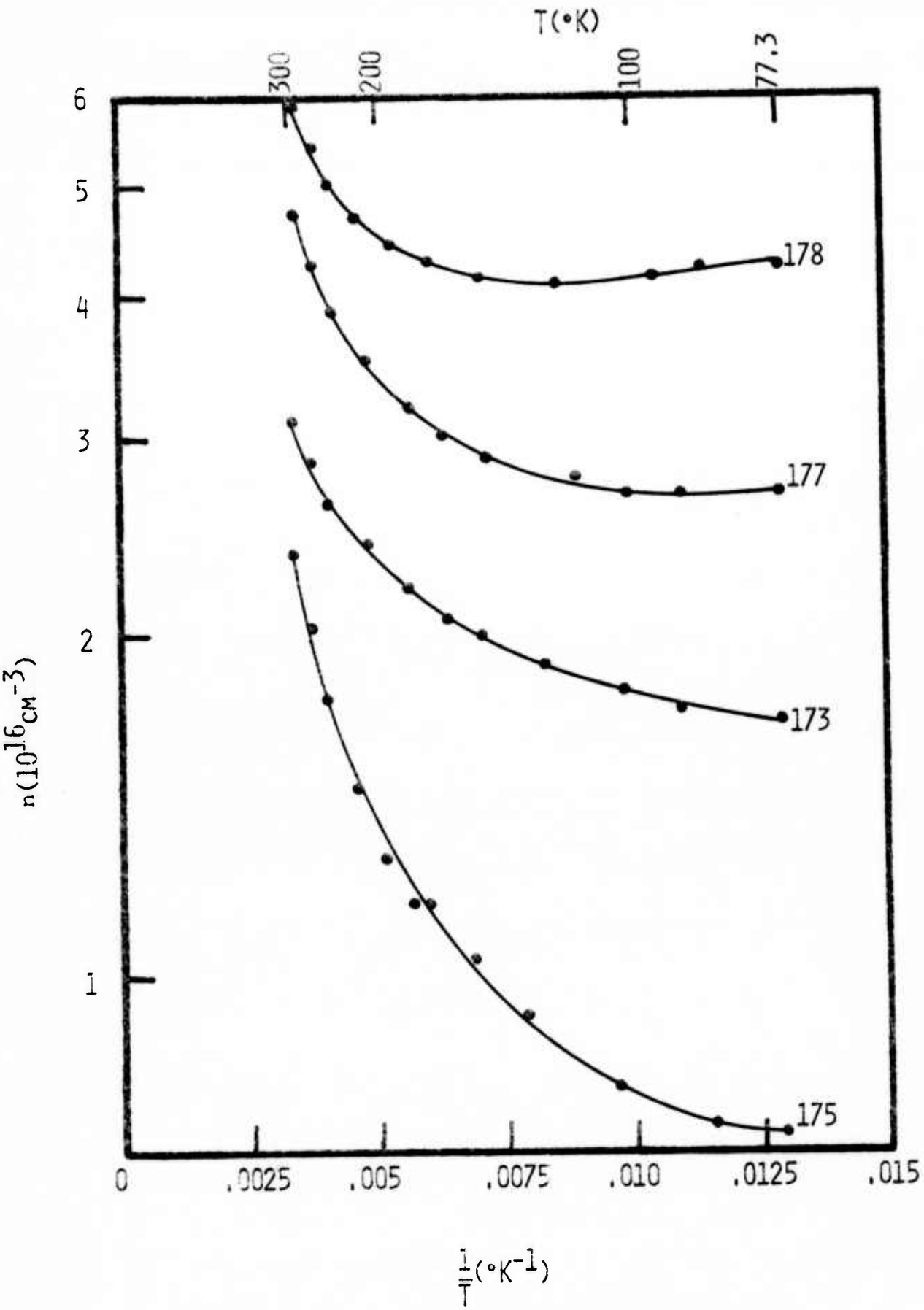

Fig. 3.14 The electron concentration as a function of the reciprocal temperature for samples 173, 175, 177 and 178, for temperatures between 77°K and 300°K.

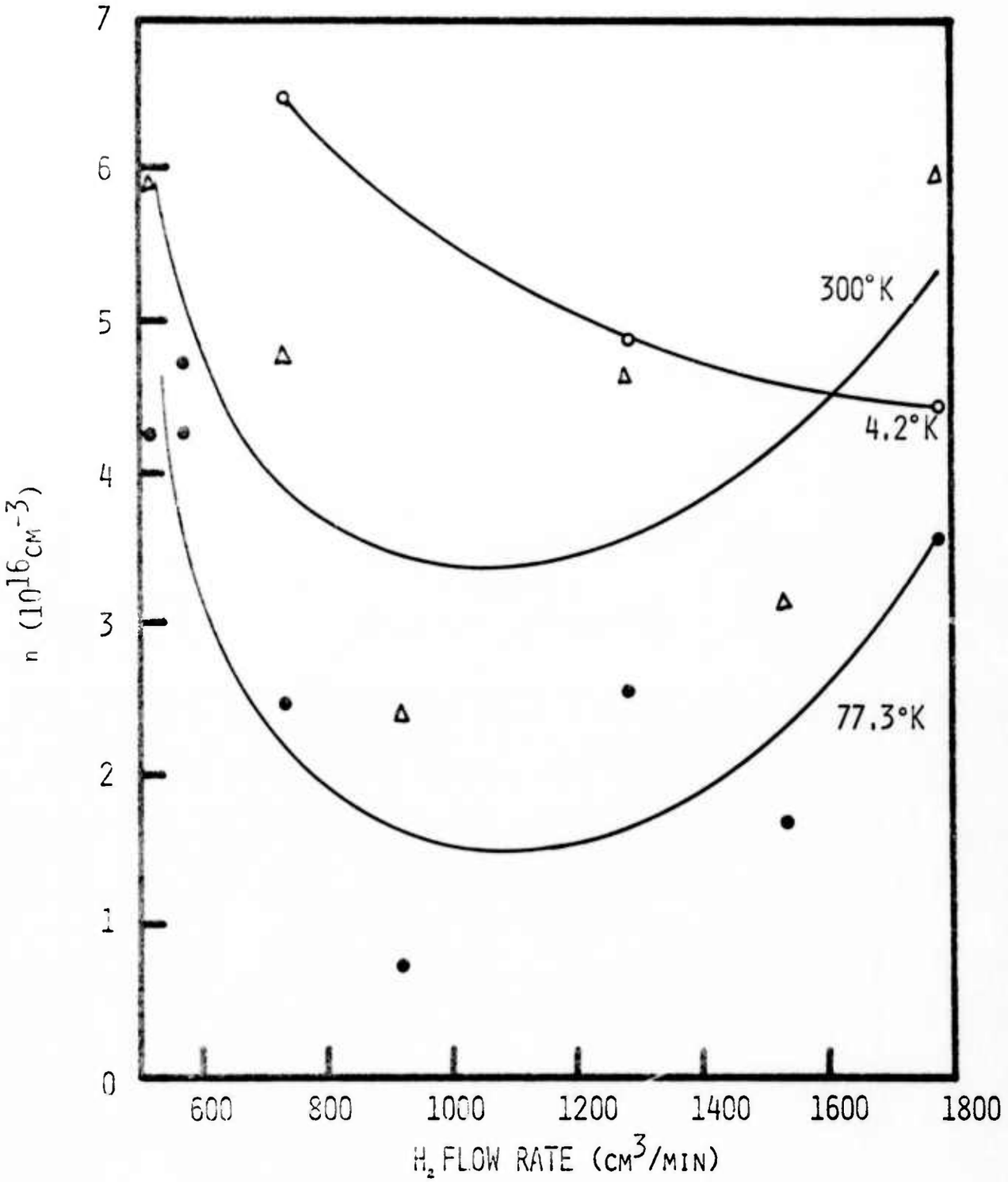

Fig. 3.15 The electron concentration as a function of the H_2 carrier gas flow rate at T = 300°K, 77°K and 4.2°K for samples 172-178.

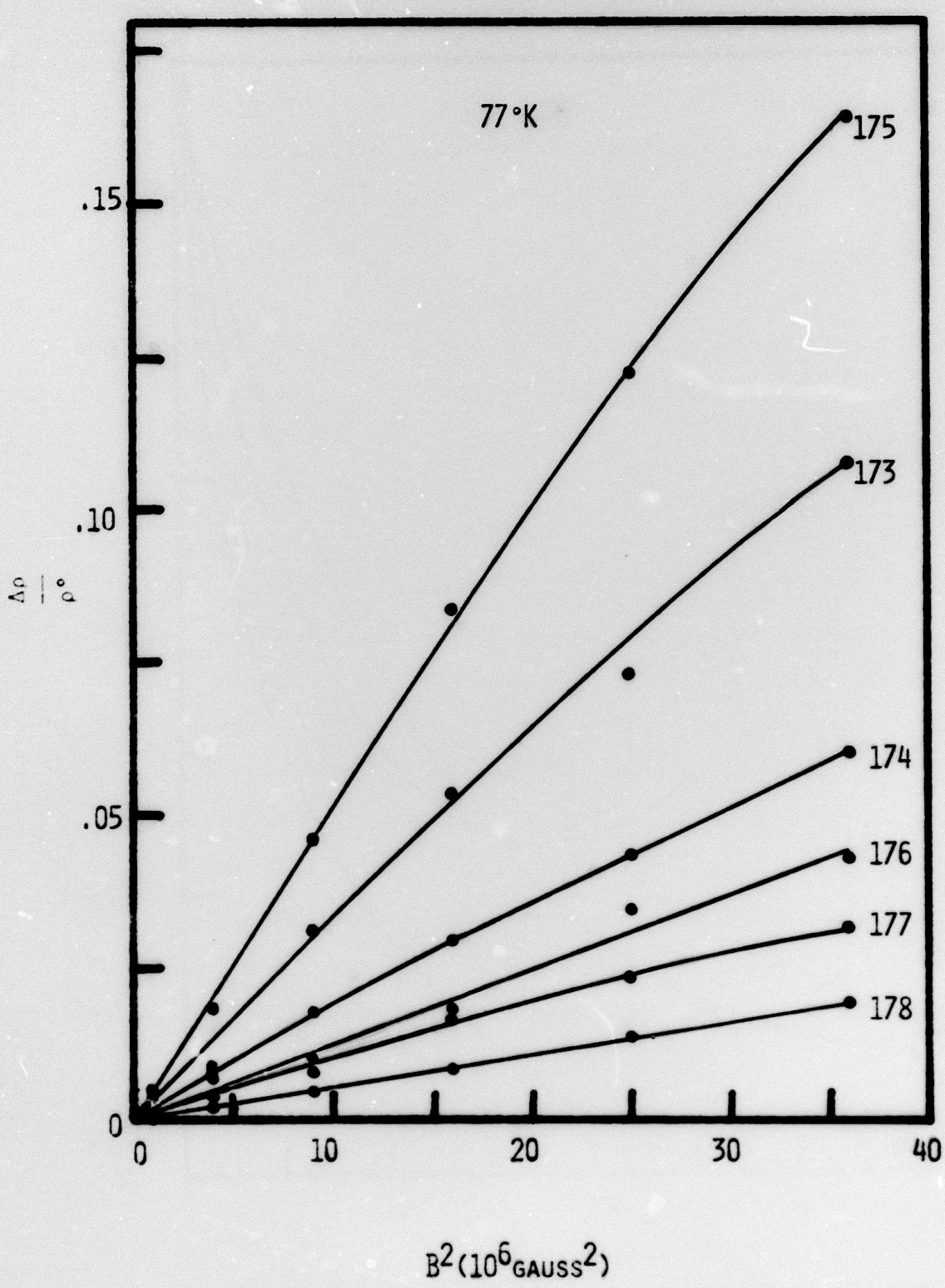

Fig. 3.16 The magnetoresistance (all positive) versus the square of the magnetic flux density for samples 173-178 at T = 77°K. A linear relationship between $\Delta\rho/\rho_o$ versus B^2 is observed for all samples at low magnetic field.

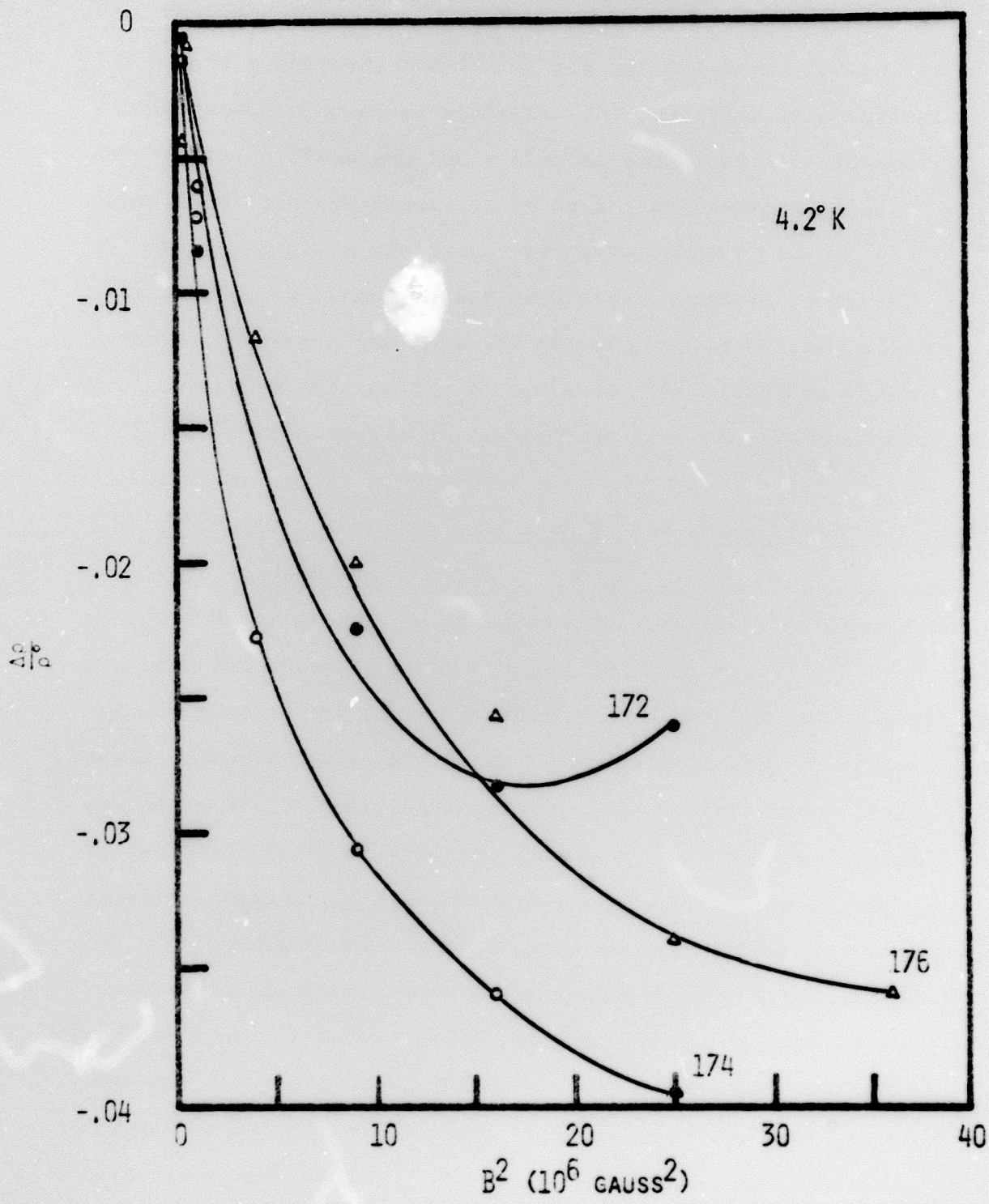

Fig. 3.17 The negative magnetoresistance versus the square of the magnetic flux density for samples 172, 174 and 176 at T = 4.2°K.

IV. OPTICAL TRANSMISSION AND SURFACE PHOTOVOLTAGE (SPV) MEASUREMENTS

In this chapter, results of the optical transmission and surface photovoltage measurements are presented. The optical absorption coefficients for epitaxial specimens 172-178 are calculated from the transmission data near the fundamental absorption edge. A review of SPV method theory for determining the minority carrier diffusion length is given. Experimental set-up for the SPV measurement is described. Preliminary results on the minority carrier diffusion length (holes in n-type specimen), as deduced from the SPV measurements, are discussed.

4.1 Optical Transmission Measurements and Absorption Coefficient Data for Samples 172-178

The experimental setup for optical transmission measurements has been described in detail in our previous report[1-2] and will not be repeated here. As pointed out in our previous report, the study of optical absorption coefficients in $InAs_{1-x}P_x$ epitaxial samples near the fundamental absorption edge, using optical transmission measurements, was severely limited. Inhibiting factors included the insufficient number of samples available, and qualitative factors such as lattice mismatching and interfacial layer effect between the GaAs substrate and the InAsP epitaxial layer. Eliminating all of these variable factors is impossible, unless destructive test procedures are employed. However, relative, rather than absolute results, will provide sufficient information to reach sound conclusions from this measurement.

Transmission measurements for epitaxial samples 172-178 were performed near the fundamental absorption edge of these samples. Absorption coefficients as a function of the wavelength were deduced from the transmission data. The results are plotted in Fig. 4.1 for samples 172-178. The resulting energy band gap deduced from the absorption edge of Fig. 4.1, for $\alpha = 10^3 cm^{-1}$, was found to vary from 0.582 eV to 0.596 eV. This result is consistent with the results of energy gap versus alloy composition displayed in Fig. 4.6 of our previous report[2].

4.2 Review of the SPV Method for Determining the Minority Carrier Diffusion Length

The most commonly used method for determining the minority carrier diffusion length, L, in a semiconductor employs a measurement of the minority carrier lifetime, τ, (e.g., by photoconductivity decay method) and the relationship $L = (D\tau)^{\frac{1}{2}}$, where D is the minority carrier diffusion constant. This method may be difficult to apply if: (1) the minority carrier lifetime is too short to measure conveniently, (2) trapping effects give misleading results for lifetime determining by photoconductive decay or similar techniques, or (3) D is not known.

The surface photovoltage technique[5] provides a unique method for determining the short minority carrier diffusion length (both in the bulk and the epitaxial semiconductor specimens) from measurement of the variation of surface photovoltage as a function of the optical absorption coefficient. Furthermore, the SPV method offers the following advantages:

(1) it does not depend upon the specific form of the relationship between the surface photovoltage and the density of the excess minority carriers (injected at the bulk edge of the surface space charge region), and (2) only capacitive contacts to the sample are needed for the measurement.

The SPV method has been widely used[5-7] to determine the minority carrier diffusion length in: (a) both the n- and p-type bulk semiconductor specimens, and (b) epitaxial layer on a thick substrate: (i) for layers with thickness greater than four diffusion lengths, the measurement yields the bulk value of L; (ii) for layers thinner than 0.5 L, the measured value is that of the substrate; (iii) for intermediate thicknesses, the bulk value of L can be estimated[7]. The SPV method, as it applies to the bulk and epitaxial semiconductor specimens, will be discussed separately as follows:

(A) Bulk Semiconductor Specimen

The surface photovoltage V_{SP} developed at the illuminated surface is a function of the excess minority carrier density, Δp, injected into the surface space charge region. The excess carrier density, Δp, is in turn dependent upon the incident light intensity, I_o, the optical absorption coefficient, α, and the diffusion length, L. The diffusion length may then be determined by measuring the variation of V_{SP} with α (i.e., wavelength, λ). An accurate knowledge of α as a function of λ is required for SPV measurement. It can be shown that the surface photovoltage may be written as[5]:

$$V_{SP} = f(\Delta p) = f\left|\frac{\eta I_o(1-R)}{(D/L)+s} \cdot \frac{\alpha L}{1+\alpha L}\right| \quad , \qquad (4.1)$$

*

where the form of the functional dependence need not be known explicitly. If η (quantum efficiency) and R (reflectance coefficient) are constant over the measured wavelength interval, Eq. (4.1) may be rewritten as

$$V_{SP} = f\left|\frac{AI_o\alpha}{(1+\alpha L)}\right| \quad , \qquad (4.2)$$

where A is a constant.

Although the specific form of this relationship may not be known, it is a monotonic function and may therefore be inverted to give

$$F(V_{SP}) = \frac{\alpha I_o}{(1+\alpha I_o)} \quad . \qquad (4.3)$$

The same value of V_{SP} may be obtained for two different values of I_o (i.e., I_{o1} and I_{o2}), provided that the corresponding values of λ and hence α are properly chosen. It follows in this case from Eq. (4.3) that

$$\frac{I_{o1}\alpha_1}{(1+\alpha_1 L)} = \frac{I_{o2}\alpha_2}{(1+\alpha_2 L)} \quad ,$$

or

$$L = \frac{[I_{o2}\alpha_2 - I_{o1}\alpha_1]}{[\alpha_1\alpha_2(I_{o1} - I_{o2})]} \quad . \qquad (4.4)$$

The minority carrier diffusion length, L, can be determined from Eq. (4.4), by measuring the light intensity, I_o, at two different wavelengths (i.e., α_1 and α_2). This would produce the same surface photovoltage, V_{SP}.

---

*where s is the surface recombination velocity and D is the diffusion coefficient.

(B) Epitaxial Semiconductor Specimen (N/N^+ or P/P^+ Structures)

For an epitaxial layer on thick substrate, the incident light intensity, I_o, required to produce a given SPV, V_{SP}, is a linear function of the reciprocal absorption coefficient, α^{-1}:

$$I_o = C\ (\alpha^{-1} + L) \quad . \tag{4.5}$$

The plot of I_o against α^{-1} has an extrapolated intercept for $I_o = 0$ at $\alpha^{-1} = -L$, from which the minority carrier diffusion length L is determined.

The minority carrier lifetime (τ) may be calculated from the measured diffusion length (L) by use of the expression $\tau = L^2/D$.

A comprehensive theoretical analysis of the SPV measurements in epitaxial semiconductor layers under various conditions has been given by Phillips[7], and will not be presented further in this section. Only the expression that is applicable to our present samples will be discussed later.

4.3 Experimental Setup for SPV Measurements

The experimental arrangement for SPV measurements is shown schematically in Fig. 4.2. The specimen surface is illuminated with chopped (13 cps) monochromatic radiation of energy slightly greater than the band gap of the semiconductor. Electron-hole pairs are produced and diffuse to the surface where they are separated by the electric field of a depletion region to produce a surface photovoltage (SPV). The SPV signal is capacitively coupled into a lock-in amplifier for

amplification and measurement. The photon intensity is adjusted to produce the same value of SPV at various wavelengths of illumination. The photon intensity required to produce this constant SPV signal is plotted against the reciprocal absorption coefficient for each wavelength. The resulting linear plot is extrapolated to zero intensity, and the negative intercept value is the effective diffusion length.

Results of SPV measurements will be included in the final technical report.

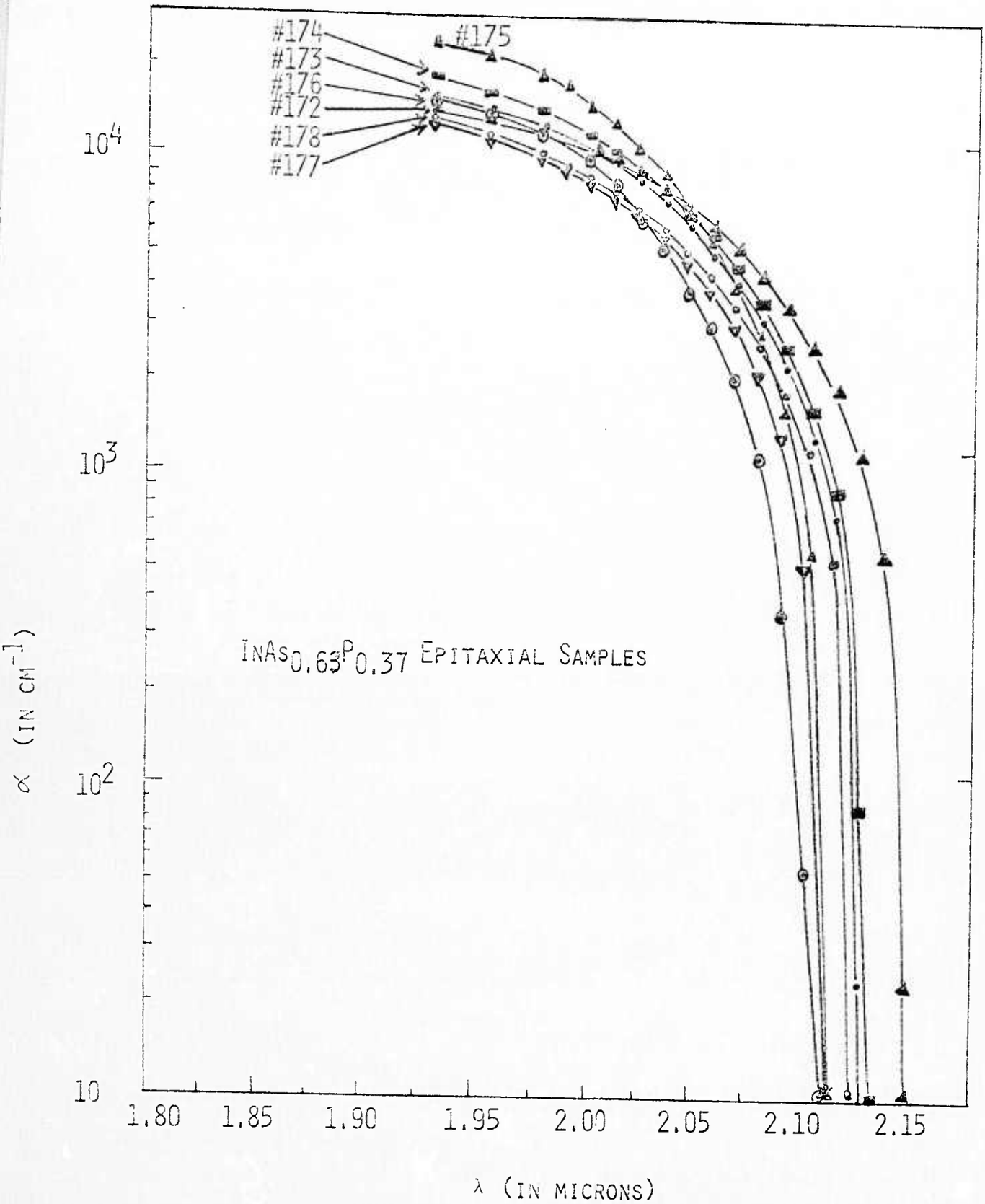

Fig. 4.1 The optical absorption coefficient versus wavelength for $InAs_{0.63}P_{0.37}$ epitaxial samples 172 through 178. The corresponding energy band for this set of samples varies from 0.586 eV to 0.592 eV.

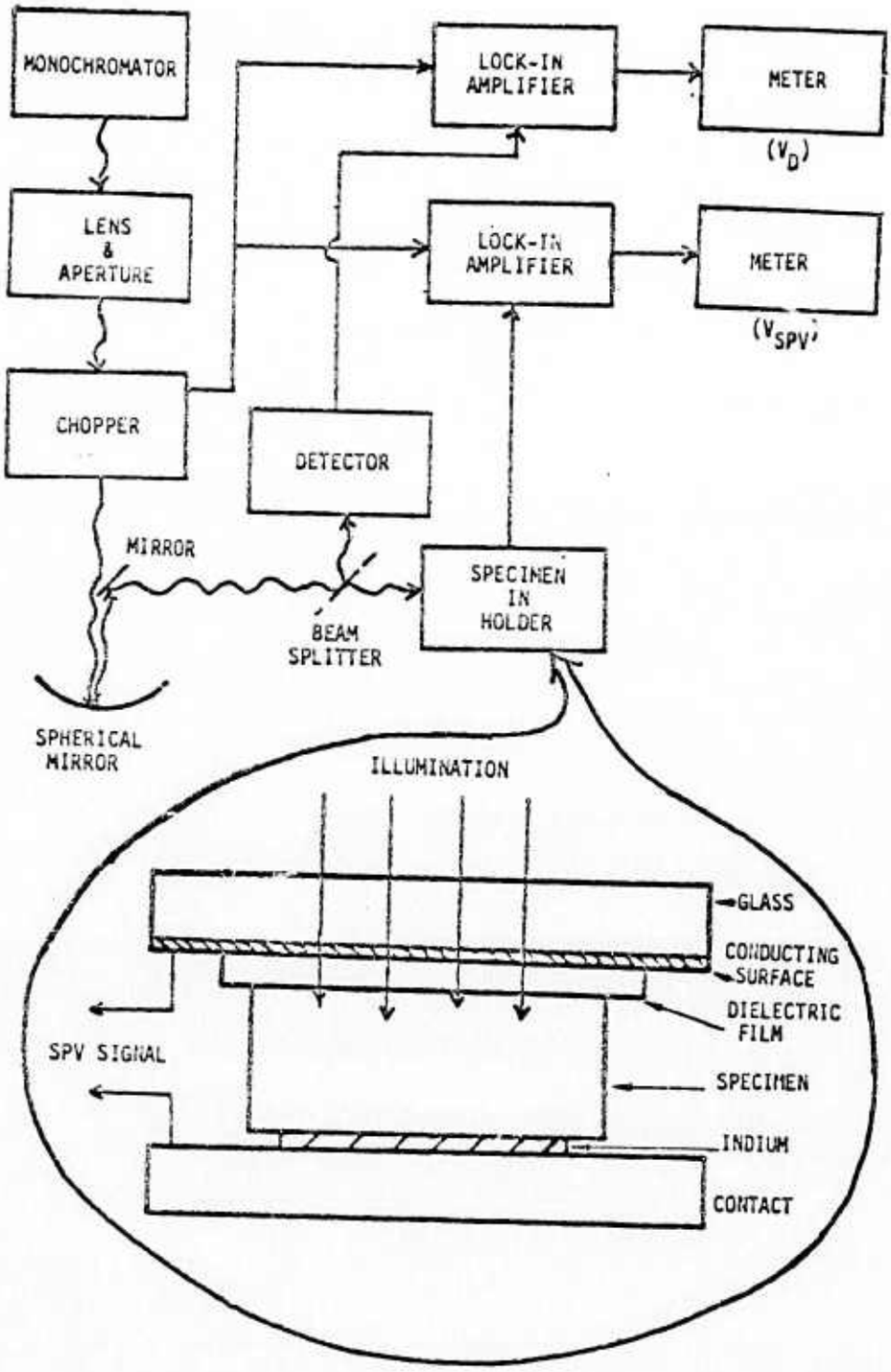

Figure 4.2 Schematic of the specimen holder for the SPV measurements and block diagram of the equipment.

V. FUTURE PLANS

Our experimental studies on the transport, optical and structural properties in both bulk and epitaxial $InAs_{1-x}P_x$ alloy systems have yielded useful information in areas such as electron mobility and electron concentration as functions of the alloy compositions, temperature, epitaxial layer thickness and the hydrogen carrier gas flow rate. The optical absorption coefficient, as a function of the wavelength near the fundamental absorption edge, has been deduced from the transmission measurements. In addition, the alloy composition has been analyzed by the electron microprobe technique. Conduction processes in the InAsP specimens have been studied, using resistivity and Hall effect measurement over the entire temperature range from 4.2°K to 300°K.

Our plans for the seventh and eighth quarters of this research contract are outlined below:

(1) Conduct photoluminescence, surface photovoltage and photoconductivity experiments to determine the band structure and recombination properties in the InAsP epitaxial samples.

(2) Assess the dominant scattering and recombination mechanisms in the InAsP alloy system, and make detailed comparison of the theoretical calculation and the experimental data on the transport and recombination parameters.

(3) Conduct studies on the transport, optical and recombination properties in the thick (50 ~ 110 μm) $InAs_{1-x}P_x$ epitaxial films grown on the semi-insulating GaAs substrate, and on the Zn-doped InAs substrates. Also, study the effect of the substrate on the transport and recombination properties in the InAsP epitaxial films.

(4) Provide concluding remarks on our study of the interrelation between varying growth parameters of InAsP epitaxial films and their effects on the transport, optical, recombination and structural properties of these specimens.

In addition to the above efforts, we plan to grow $Ga_xIn_{1-x}As$ epitaxial films on InP substrate, and study the electronic transport properties in these films.

VI. REFERENCES

1. S. S. Li, "Investigation of Basic Electronic Transport, Recombination and Optical Properties in $InAs_{1-x}P_x$ Alloy Systems," 1st Semi-Annual Technical Report, Contract No. DAAK02-74-C-0102, Night Vision Laboratory, June 15 (1974).
2. S. S. Li, "Investigation of Electronic Transport, Recombination and Optical Properties in $InAs_{1-x}P_x$ Alloy Systems," 2nd Semi-Annual Technical Report, Contract No. DAAK02-74-C-0102, Army Night Vision Laboratory, December 15 (1974).
3. E. A. Davis and W. D. Compton, "Compensation Dependence of Impurity Conduction in Antimony-Doped Germanium," Phys. Rev., vol. 140, p. A2183 (1965).
4. A. Miller and E. Abrahams, "Impurity Conduction at Low Concentrations," Phys. Rev., vol. 120, 745 (1960).
5. A. M. Goodman, J. Appl. Phys., vol. 32, p. 2550 (1961).
6. E. O. Johnson, Phys. Rev., 111, p. 153 (1959).
7. W. E. Phillips, Solid State Electronics, vol. 15, p. 1097 (1972).